






Article

Global Events and Surge in Residential Water Demand: Exploring Possible Hydraulic Scenarios

Holger Manuel Benavides-Muñoz ¹, Mireya Lapo-Pauta ¹, Francisco Javier Martínez-Solano ^{2,*},
Manuel Quiñones-Cuenca ^{1,3} and Santiago Quiñones-Cuenca ¹

- ¹ Research Group R&D for the Sustainability of the Urban and RURAL Water Cycle, Civil Engineering Department, Universidad Técnica Particular de Loja, Loja 110107, Ecuador; hmbenavides@utpl.edu.ec (H.M.B.-M.); cmlapo@utpl.edu.ec (M.L.-P.); mfquinonez@utpl.edu.ec (M.Q.-C.); lsquinones@utpl.edu.ec (S.Q.-C.)
- ² Department of Hydraulic Engineering and Environment, Universitat Politècnica de València, 46022 Valencia, Spain
- ³ Computer Science and Electronics Department, Universidad Técnica Particular de Loja, Loja 110107, Ecuador
- * Correspondence: jmsolano@upv.es

Abstract: For humankind to survive, access to sufficient and safe drinking water is fundamental. This study explores the connection between rising domestic water consumption and planetary phenomena, such as rapid population growth, climate change, and pandemics. To achieve the study's objectives, it provides a thorough forecast of water use, considering probable global scenarios for the years 2030 and 2050. The modeling approach is adapted from a consistent case study taken from the body of scientific literature on water supply hydraulics. The study's results highlight the necessity for proactive and flexible management strategies for water resources. Notably, it observes significant alterations in water supply management to adjust water allocation due to the unanticipated and ongoing increase in consumer demand. The forecasted scenarios indicate potential difficulties that may arise in meeting rising domestic water demand amid planetary phenomena. The presented results offer valuable insights to policymakers and water supply authorities, enabling them to effectively address the rising domestic water demand while considering potential adverse conditions, ensuring a sustainable water supply for future generations.



Citation: Benavides-Muñoz, H.M.; Lapo-Pauta, M.; Martínez-Solano, F.J.; Quiñones-Cuenca, M.; Quiñones-Cuenca, S. Global Events and Surge in Residential Water Demand: Exploring Possible Hydraulic Scenarios. *Water* **2024**, *16*, 956. <https://doi.org/10.3390/w16070956>

Received: 9 February 2024
Revised: 13 March 2024
Accepted: 20 March 2024
Published: 26 March 2024



Copyright: © 2024 by the authors. Licensee MDPI, Basel, Switzerland. This article is an open access article distributed under the terms and conditions of the Creative Commons Attribution (CC BY) license (<https://creativecommons.org/licenses/by/4.0/>).

Keywords: demand patterns; consumption curves; pressure management; water meter error; COVID-19

1. Introduction

Access to potable water and a healthy environment is an inherent right of human beings. Despite experiencing a declining growth rate and falling fertility, the world's populace continues to increase [1], leading to higher demands on water supply systems. In 2012, the United Nations [2] estimated that the global population would reach a value that could stabilize around 9 billion inhabitants by the year 2050. UN WATER [3] reported that the population is growing at a rate of 80 million people per year and is projected to reach 9.1 billion people by 2050. It further warns that population growth, urbanization, industrialization, increasing consumption, and production will result in an ever-growing demand for water.

The increase in the world's population also escalates the need for water among people, necessitating the adoption of sophisticated methods to extract, transport, and ensure the safety of water for consumption. According to UN-WATER [4], demographic and economic growth will lead to a 55% increase in water demand between the period 2017 and 2040.

Another phenomenon impacting the planet is climate change, manifested as increased variability in the water cycle, leading to extreme weather events, heightened uncertainty in water availability, and endangering ecological balance [5]. It restricts biodiversity

and hampers humans' ability to enjoy their rights to uncontaminated water and a clean environment worldwide.

Ensuring urban water security is paramount for achieving resilience in future smart cities, especially under the impact of climate change and socio-economic factors, which even jeopardize the sustainability of water resources [6].

The challenge of meeting future water demand due to increased water stress will require increasingly difficult decisions regarding the allocation of natural water sources among competing water consumption groups [5].

To create a sustainable future, the "status quo" must change, and the requirements of water conservation measures need to be examined via a lens capable of addressing the stress caused by a system of increasing and ever-more-critical change, where around 800 million people currently lack access to vital basic services [7]. UN-WATER [8] indicates that in dealing with the present and future water challenges, it is essential to employ inventive and transformative concepts, adopting a "beyond business as usual" approach.

Based on the foundation of the aforementioned recommendations and the proposed approach of employing innovative and transformative concepts [3–8], this study focuses on considering planetary impact phenomena, such as population growth, climate change, and pandemics, which have the greatest influence on the increase in residential water consumption, primarily. The study aims to assess the impact of these factors on the functionality of water distribution networks. An estimation of water consumption increases was developed by combining potential demand scenarios for the years 2030 and 2050.

In order to assess the effect of changing demands, a study was carried out on a well-known network model (Anytown, Walski et al. [9]). This model was used to study the water supply system, exploring the variation in the consumption factor (FQ). This investigation applied a combination of fundamental scenarios, encompassing potential future operating and functional conditions of the network, including population growth, climate change, pandemics, wildfires, and variations in hourly demand (peak demand). Among the findings, notable increases in energy requirements to meet the projected future domestic water demands are evident.

2. Methodology

Simulations, categorized into seven combinations and two scenarios (2030 and 2050), explore various factors influencing water demand, including fundamental combinations for increasing the water consumption factor (FQ). These factors encompass peak consumption [3], variations in hourly demand, impacts of climate change [4], and potential increases in demand due to the effects of pandemics (estimated at 10% for a scenario similar to the COVID-19 (SARS-CoV-2) event and 40% for a hypothetical future pandemic caused by the patented SARS-CoV-3 [10], which is assumed to result in up to four times higher water consumption, deemed improbable at this moment). This assessment also aligns with the value indicated by Alda-Vidal et al. [11]. Additionally, simulations consider population expansion and fire events that can be mitigated via the same network.

Corroborating evidence from various studies, such as the 8.08–16.41% increase in hot water demand in the residential sector due to COVID-19 [12], a 17% rise in hourly water usage during lockdown [13], an average water consumption increase ranging from 8.5% to 13.2%, with a 19.8% absolute rise in consumed water [14], and a projected hypothetical increase of 40%, and the unprecedented challenges brought to public drinking water systems [15], provides additional insight into these scenarios. Acknowledging the diverse literature on this subject, encompassing studies with contrary results and varying durations of analysis is crucial for a comprehensive understanding of the projected increase [16]. Further exploration into specific regional impacts, including the 8.5% overall water demand increase in Salt Lake County in 2020 [17], disruptions in California's urban water consumption during stay-at-home orders [18], and changes in water consumption patterns in northern Germany [19], underscores the nuanced effects of the pandemic on water utilities. The comprehensive discussion on five Apulian towns [20] and the broader

impact on U.S. utilities [21] emphasizes the necessity for adaptive measures and careful consideration of potential negative consequences in future infrastructure planning, providing valuable insights to guide future preparedness, regulation, resilience, and communication strategies [15,22].

2.1. Description of the Combinations and Scenarios

The examination thoroughly investigated the most significant factors and their impact on water consumption within each of the seven combinations (A to G) and two scenarios (2030 and 2050). Modeling realistic future water consumption patterns involved considering historical trends, demographic patterns, climate projections, and other relevant elements. The modeling methodology allowed for the evaluation of potential issues brought on by rising water demand as well as the exploration of strategies for managing the water supply sustainably under different conditions.

By describing and evaluating these diverse scenarios, this study provides valuable insights into the complex interactions between population growth, climatic changes, pandemic impacts, and other variables affecting water demand [23]. The results highlight the significance of developing flexible strategies to meet the difficulties of increasing water demand and maintaining the resilience of water delivery systems in urban areas.

2.1.1. Peak Water Consumption

Peak water consumption represents the highest level of water usage observed in a water supply system during a specific period, typically during periods of high demand. To estimate peak water consumption, historical data on water usage patterns and peak demand events were analyzed, considering factors such as seasonal variations, climatic conditions, and specific consumption patterns [23,24]. The UN WATER [3] report and relevant studies on peak water demand were utilized as a foundation for estimating future peak consumption. Understanding the factors that influence water consumption and providing technical evidence of individual use for enhanced water demand projection would assist developing, emerging, and low-income countries in securing a sustainable urban water supply [25].

The estimation of peak water consumption (Q_{peak}) is typically performed using Equation (1):

$$Q_{peak} = Q_{avg} \times P_p \quad (1)$$

where Q_{peak} represents the peak water consumption (in liters per second); this quantity is also known as the Maximum Hourly Flow in the criteria for design or specifications of some countries [26]. Q_{avg} denotes the average water consumption during non-peak periods (in liters per second). P_p signifies the peak demand factor, which is a dimensionless ratio indicating the multiplier applied to the average consumption to account for peak periods.

The peak demand factor (P_p) is derived from the local regulations in each country and is the result of rigorous analysis of historical data. Additionally, it mentions that the P_p value may change depending on various factors, such as the time of day, day of the week, weather, and specific events that increase water usage [27].

2.1.2. Water Consumption Due to Climate Change— Q_{cc}

Climate models and predictions were utilized to anticipate future changes in temperature and precipitation patterns, evaluating the effects of climate change on water use. Following that, these modifications were used to forecast potential changes in water demand [28], considering factors such as accelerated evaporation rates, altered vegetation patterns, and expected alterations in seasonal water supply. This research was influenced by the UN WATER [4] report and other climate change effect assessments.

The expected rise in global temperature is a key factor in estimating future water use. The average world temperature is predicted to increase by 1.5 degrees Celsius over pre-industrial levels between 2030 and 2035, mostly as a result of human activity, according to the Intergovernmental Panel on Climate Change (IPCC) of the United Nations (UNDP) [6].

Additionally, the five years from 2016 to 2020 have been recorded as the hottest since at least 1850, demonstrating the continuous high rate of warming [6]. At the current pace of warming, the world could surpass the critical 1.5 °C threshold even before 2050, possibly as early as the 2030s. Experts on Climate Change, following the Paris Climate Summit, have warned that by 2050, the planet could be experiencing a two-degree Celsius increase in temperature [29,30].

The alarming predictions underscore the urgent need to estimate water consumption, considering the cumulative impact of global temperature rise. By incorporating the temperature increase into the equation predicting water use via integrals, we can better anticipate the growing demand for water due to climate change [31]. This approach empowers decision-makers and water authorities to devise more effective and adaptable strategies for sustainable water resource management, ensuring a continuous and sustainable water supply in light of the escalating effects of climate change.

The water consumption equation can employ Equation (2) to describe the cumulative impact of temperature changes over time in order to account for the anticipated rise in global temperature. Let t be the number of years from the current year, and let $T(t)$ be the function reflecting the global temperature at that time.

$$Q_{cc}(y) = Q(0) \left(1 + \frac{\Delta t}{100} \right) \left(1 + \int_0^t T(y) dy \right) \quad (2)$$

where $Q_{cc}(y)$ represents the projected water consumption at time y years from the current year. $Q(0)$ is the current water consumption. Δt is the desired percentage increase in water consumption at time t (per year). $T(y)$ is the function representing the global temperature at time s years from the current year. $\int_0^t T(y) dy$ is the integral of the global temperature function from 0 to t , representing the cumulative temperature change over time. See Appendix A.

2.1.3. Water Consumption Due to SarsCoV; Q_{cov10} and Q_{cov40} Increase

The COVID-19 epidemic had a noticeable effect on how people behaved and how much water they used. Data on variations in water demand during lockdowns, cleanliness habits, and increased household activities were taken into consideration to support the 10% rise in water consumption during the pandemic. This estimate was supported by comparisons of pre- and post-pandemic water usage patterns from dependable sources like Alda-Vidal et al. [11], Kim et al. [12], Jia et al. [13], Kasak [14], Sowdy and Hansen [17], Lüdtke et al. [19], Kalbusch et al. [32], Nemati and Tran [33], Gholami et al. [34], Buurman et al. [35], and Birisci and Ramazan [36]. The estimation of a hypothetical future outbreak, triggered by the already patented SARS-CoV-3 virus [10], allows for the current simulation with the projection of this higher estimate of 40% per pandemic [11], even though it may currently be deemed improbable. See Figure 1.

The water demand projections, estimating the most significant lower and upper average percentages, are considered for this study at 10% and 40%, respectively, based on previous studies and hypothetical considerations [11–14,17,19,20,32–37].

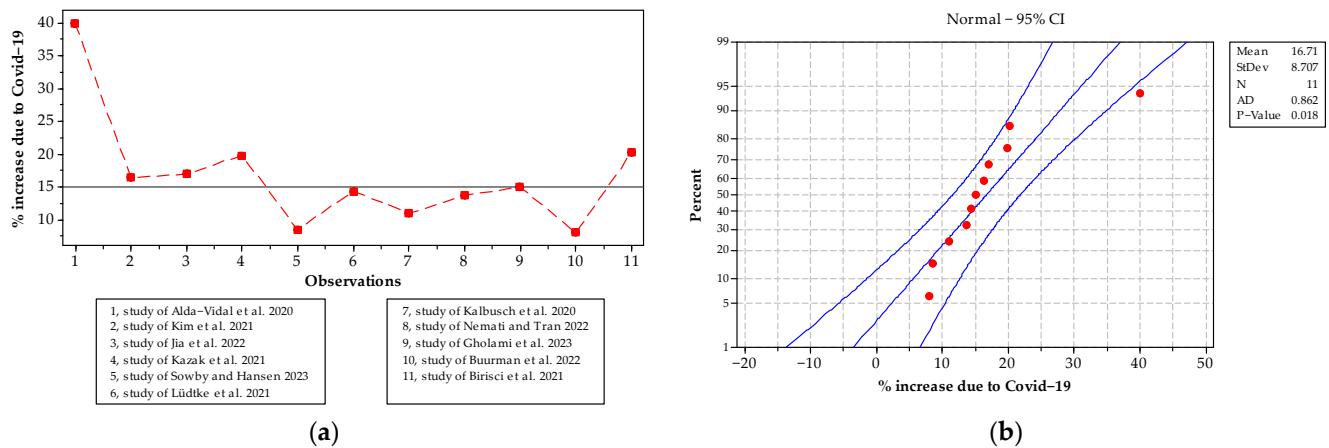


Figure 1. Graphical analysis of COVID-19's impact on water demand: probability plot and run chart of daily maximum percentage increase [11–14,17,19,32–36] (a) run chart of % increase in demand for water due to COVID-19; the figure displays a run chart illustrating the distribution of percentage increases in water demand attributed to COVID-19. Key findings include the number of runs about the median: 3. Expected number of runs: 6.45455. Longest run about the median: 6. Approximate p value for clustering: 0.01334. Approximate p -value for mixtures: 0.98666. Number of runs up or down: 8. Expected number of runs: 7. Longest run up or down: 2. Approximate p -value for trends: 0.78303. Approximate p value for oscillation: 0.21697. *Interpretation:* The number of runs around the median is less than the expected number, indicating some degree of clustering. The number of runs up or down is greater than expected, suggesting some trend or variability in the data series. The longest run around the median and up or down is 6 and 2, respectively. p -values indicate significant evidence of clustering ($p = 0.01334$) and no significant evidence of oscillation ($p = 0.21697$). The (a) suggests significant patterns in the distribution of percentage increases in water demand due to COVID19, with some clustering and trends in the data. (b) Probability plot of % increase in daily maximum water demand due to COVID-19; the figure depicts a probability distribution of percentage increases in daily maximum water demand attributed to COVID-19. Based on 11 observations, the plot reveals a mean of 16.71% and a standard deviation of 8.707. The Anderson–Darling test statistic (AD) is 0.862, with an associated p -value of 0.018. These findings suggest a departure from normal distribution, as the p value falls below the commonly used significance threshold of 0.05. The deviation from the normal model is supported by the relatively high AD statistic. The (b) indicates that percentage increases in daily maximum water demand due to COVID-19 do not conform to a normal distribution. The Lower Bound and Upper Bound lines represent both limits of the 95% confidence interval for the normal distribution fitted to the data of the % increase due to COVID-19. These bounds illustrate the expected variability around the best-fit line and provide a measure of the certainty of parameter estimation for the normal distribution. A wider confidence interval indicates greater uncertainty in estimating the distribution parameters.

2.1.4. Water Consumption Due to Population Growth— Q_{PG}

To estimate the increase in water consumption due to population growth in urban networks, Equation (3) can be used.

$$Q_{PG}(y) = \int_{t_0}^{t'} P'(y) dy \cdot \int_{t_1}^{t'} C'(y) dy \quad (3)$$

where $Q_{PG}(y)$ represents the projected water consumption at time (y) due to population growth, $P'(y)$ is the projected global population at time (t), t_0 is the baseline year, $C'(y)$ is the per capita water consumption rate at time t' , and t_1 is the present time (baseline) when the population and per capita water consumption rates are known. t' is the future year in which the water consumption is projected. See Appendix B.

Reliable sources like the World Population Prospects 2022 report from the United Nations [38] provide population increase forecasts. The projection of future water consumption heavily relies on estimates of the size of the world's population and its yearly growth rate for the period 1950–2022, as well as the medium scenario and 95% prediction intervals for the years 2022–2050.

The World Water Development Report [22] and The World Population Prospects 2022: Summary of Results [38] were studied to validate the estimated increases in water consumption due to population growth for both the years 2030 and 2050. See Table 1.

Table 1. Values of the increase in consumption factor FQ.

Variable	Description	2030	2050
Q_{peak}	Peak Consumption	1.330	1.5500
Q_{cc}	Climate Change Consumption-CC	0.310	0.7890
Q_{cov10}	COVID-19 Consumption; 10% Increase	0.100	0.1000
Q_{cov40}	Cov40 Consumption; 40% Increase	0.400	0.4000
Q_{PG}	Population Growth Consumption-CP	0.132	0.3158
Q_F	Fire Consumption. N13, Ke = 9	Q_e	Q_e

Note: Industrial demand is not included in this analysis.

2.1.5. Water Consumption Due to Fire— Q_F

The estimation of water consumption related to fire incidents was based on assessments of the fire hazard, which took into account variables such as fire frequency, severity, and the potential area affected. Hydraulic analyses were used to determine the emitter coefficient (Q_F) for fire hydrant activations, considering the water flow required to combat different types of fires and the distance covered by water jets. The selected emitter coefficient of 9 and emitter exponent of 0.5 were determined via investigations and previous fire flow analysis models [27,39,40]. The node location (N13) considered in this analysis was selected as a representative scenario studied in Cunha and Sousa [41] and other relevant research on fire protection in water supply systems.

The summary of the variables considered and the combinations applied for this study is presented in Tables 1 and 2.

Table 2. Combination of water consumption for key global phenomena.

Combination Identifier	Variable Combination (Summation)	FQ Analysis	FQ Analysis	Pressure Minimum	Pressure Desirable
		2030	2050	(m)	(m)
G	Q_{peak}	1.330	1.550	20	30
F	$Q_{peak} + Q_{cc}$	1.640	2.339	20	30
E	$Q_{peak} + Q_{cc} + Q_{cov10}$	1.740	2.439	15	25
D	$Q_{peak} + Q_{cc} + Q_{cov10} + Q_{PG}$	1.872	2.755	15	20
C	$Q_{peak} + Q_{cc} + Q_{cov40} + Q_{PG}$	2.172	3.055	15	20
B	$Q_{peak} + Q_{cc} + Q_{cov10} + Q_{PG} + Q_F$	$1.872 + Q_F$	$2.755 + Q_F$	10	15
A	$Q_{peak} + Q_{cc} + Q_{cov40} + Q_{PG} + Q_F$	$2.172 + Q_F$	$3.055 + Q_F$	10	15

2.2. Case Study

This study investigates a water distribution system of a hypothetical community, Anytown, U.S.A., similar to that described by Walski et al. [9]. The system draws water from a nearby river, treats it at a central plant, and employs three parallel pumps to distribute the water from the clearwell. Walski's study revealed that the system was initially developed in 1910, using old cast iron pipes with low Hazen-Williams C-factors. After World War II, the town expanded toward the northwest and west, facing challenges with a newly erected tank and the possibility of a new industrial park to the north. To meet future demands until 2005, the city planned water distribution system upgrades.

The study focused on selecting new pipes, pumps, and tanks while considering existing pipes needing cleaning and lining to meet pressure requirements at the lowest cost. The analysis used projected C-factors for 2005, and average daily water use and node elevations for 1985 and 2005 were examined. The system had to maintain a minimum pressure of 40 psi at all nodes during peak flow and at least 20 psi while meeting fire flow requirements. Fire flow varied for different nodes, and the system had to meet these demands while supplying peak day flows. The comprehensive analysis seeks to contribute to sustainable water resource management and enhance urban water supply systems' resilience to various demands and uncertainties [9].

By testing on the Anytown, USA network, this study analyzes the network's behavior for different flow rates, which are increased based on the possible combinations of consumption patterns according to the proposed study scenarios. It aims to address water distribution system challenges and provide insights for optimizing urban water supply networks. The network's complexity reflects real-world systems, making it a suitable workbench. The study aims to enhance water resource management and the resilience of urban water supply systems in the face of uncertainties.

The Anytown, USA network has been subject to investigation and analysis by Lansey et al. [42], Xu and Goulter [43], and further examination by Cunha and Sousa [41], among other researchers. This study also utilizes the same network to analyze and research water distribution system challenges and optimize urban water supply networks.

In this case study, instead of the three identical pumps installed in parallel, which initially suction water from the river to the central treatment plant (as proposed by Walski et al. [9]), the network includes an injection tank at an elevation of 55 m. This tank supplies 15 nodes at an elevation of 0 m with a consumption rate of 43.89 L/s. The nodes are connected by 33 hydraulic lines, forming 18 basic loops. Node 1 is considered to have no consumption in the analysis. See Figure 2. The characteristics of the hydraulic lines in the network are detailed in Table 3.

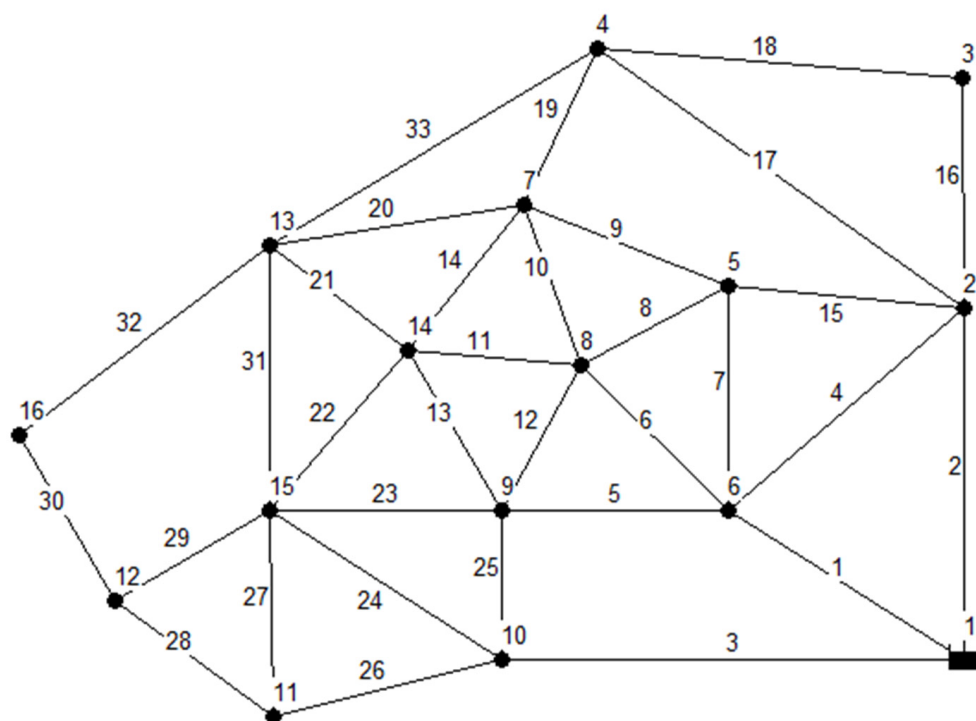


Figure 2. Graphical representation of the meshed network under study. Numbers represent nodes and links IDs.

Table 3. Characteristics of the hydraulic lines in the studied network.

ID	Length (m)	Diameter (mm)	ID	Length (m)	Diameter (mm)
Pipe 1	3660	200	Pipe 17	2740	250
Pipe 2	3660	500	Pipe 18	1830	100
Pipe 3	3660	600	Pipe 19	1830	100
Pipe 4	2740	100	Pipe 20	1830	100
Pipe 5	1830	100	Pipe 21	1830	100
Pipe 6	1830	100	Pipe 22	1830	250
Pipe 7	1830	100	Pipe 23	1830	100
Pipe 8	1830	250	Pipe 24	1830	500
Pipe 9	1830	250	Pipe 25	1830	250
Pipe 10	1830	100	Pipe 26	1830	200
Pipe 11	1830	100	Pipe 27	2740	100
Pipe 12	1830	100	Pipe 28	1830	125
Pipe 13	1830	100	Pipe 29	1830	350
Pipe 14	1830	100	Pipe 30	1830	300
Pipe 15	1830	400	Pipe 31	1830	250
Pipe 16	1830	250	Pipe 32	3660	100
			Pipe 33	3660	100

Notes: The hydraulic lines of the model are grouped into three types of length: lines 1 to 3, 32, and 33 have a length of 3660 m; hydraulic lines number 4, 17, and 27 have a length of 2740 m; and hydraulic lines 5–16, 18–26, 28–31 have a length of 1830 m.

3. Results

When the network is just required to fulfill the flow demand to $FQ = 1.0$, the first scenario (basic) takes place. An injection node head of 55 m is required to meet this demand. Thus, by 2030, the minimal pressure (N6) is available at a height of 30.29 m, and by 2050, the minimum pressure occurs at node N4 with a height of 21.25 m. Additionally, a total flow of 658.33 L/s is required from the injection tank when the emitter is closed.

To determine the scenario with the most probable combination, the principle of Simulated Annealing was employed. The Optimization Heuristic using the Simulated Annealing technique, proposed by Kirkpatrick [44], Kirkpatrick et al. [45], Kirkpatrick [46], and later by Černý [47], was chosen due to its demonstrated effectiveness in various situations, as supported by Van Laarhoven et al. [48], Millán-Páramo et al. [49], and Naidu et al. [50]. Figure 3 shows the flowchart corresponding to the Simulated Annealing Heuristic Optimization algorithm used for this analysis.

The Simulated Annealing [45–47] algorithm initiates with a high initial temperature $T_1 = 94$, facilitating extensive exploration of the solution space. This temperature gradually decreases with each iteration using a cooling factor of 0.85, enabling the algorithm to exploit favorable local optimal solutions as it cools.

The cooling schedule can take a geometric or exponential form, with typical cooling factors ranging from 0.80 to 0.99. A cooling factor of 0.85 was chosen to balance exploration (due to the high initial temperature) and exploitation (emphasizing good solutions as the temperature decreases).

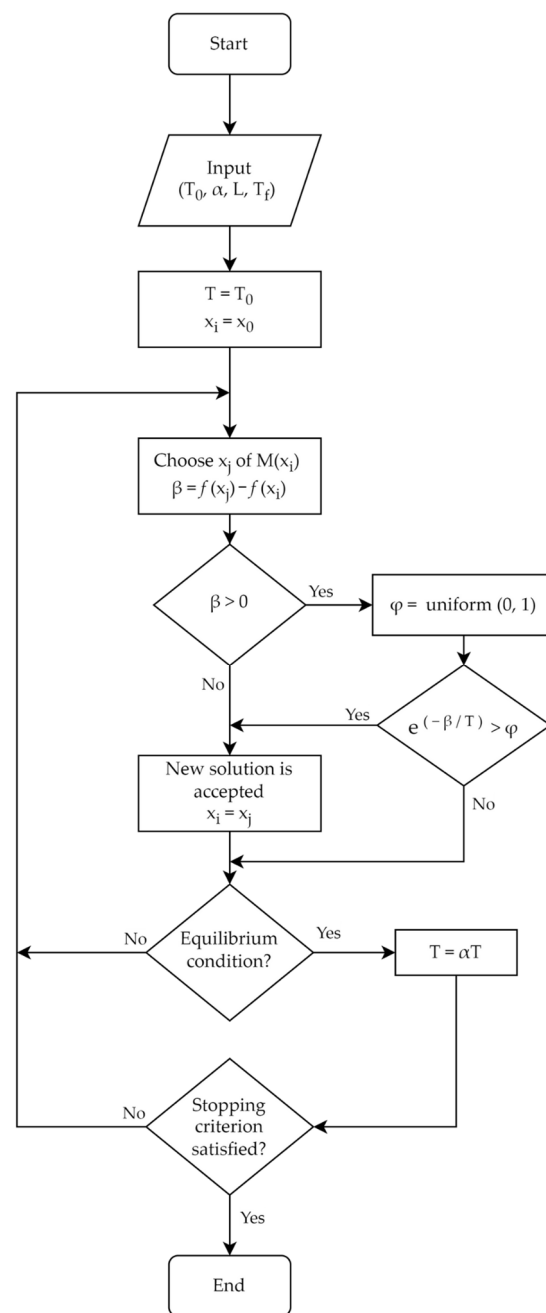


Figure 3. Flowchart: Simulated Annealing Heuristic Optimization algorithm.

The Simulated Annealing implementation utilized a geometric cooling schedule with a factor of 0.85 to strike a balance between exploration and exploitation. Other specifications included a temperature change (L) of 1 at each iteration, a step size/radius of 1, and an initial temperature (T_1) of 94. Executing the algorithm with these parameters yielded the subsequent iterative temperature schedule: 94.00, 79.90, 67.92, 57.73, 49.07, 41.71, 35.45, very similar to the outcomes achieved by Cunha and Sousa [41]. This gradual temperature decrease allows for extensive exploration of the solution landscape initially, transitioning to focus on locally optimal scenarios based on the probabilities presented in the table below. The high initial temperature facilitates thorough exploration, with subsequent declines enabling the algorithm to converge on combinations with a higher likelihood of occurrence out of the seven scenarios analyzed. The results of this adaptation are presented in Table 4.

Table 4. Probabilities of occurrence for consumption scenarios.

Combination	G	F	E	D	C	B	A	Probable FQ2030 (%)	Probable FQ2050 (%)
Scenario 2030	1.330	1.640	1.740	1.872	2.172	1.895	2.196		
Scenario 2050	1.550	2.339	2.439	2.755	3.055	2.770	3.070		
1	94.00	1.00	1.00	1.00	1.00	1.00	1.00	136.53	162.13
2	79.90	3.35	3.35	3.35	3.35	3.35	3.35	144.84	178.88
3	67.92	5.35	5.35	5.35	5.35	5.35	5.35	151.90	193.11
4	57.73	7.05	7.05	7.05	7.05	7.05	7.05	157.90	205.22
5	49.07	8.49	8.49	8.49	8.49	8.49	8.49	163.00	215.51
6	41.71	9.72	9.72	9.72	9.72	9.72	9.72	167.33	224.25
7	35.45	10.76	10.76	10.76	10.76	10.76	10.76	171.02	231.69

Table 4 shows the probability distribution over the two scenarios (2030 and 2050) at each temperature level. As the temperature decreases, the probability mass shifts toward the optimal Scenario 1. At the highest initial temperature of 94, Scenario 1 has 94% probability, with the remaining scenarios having 1% each.

As the temperature cools to 35.45, the probability of Scenario 1 increases to 162.13% of the initial 94% value. The other scenarios now have a 10.76% probability each. This represents exploitation and intensification around the optimal Scenario 1 solution.

The FQ Probable (Probable Q(flow) Factor) denotes percentages that signify the growth multiples in probability versus the initial probabilities for each scenario. For the 2030 forecast, the 136.53% FQ Probable value for Scenario 1 represents a final likelihood of 128.34% after optimization. For the 2050 prediction, Scenario 1 has an FQ Probable of 162.13%; when applied to the original 94.00% probability, this results in a final likelihood of 152.40% for Scenario 1 after optimization. The highest FQ Probable percentages indicate the algorithm successfully exploring the solution landscape and exploiting improved combinations for the presented consumption model in both the 2030 and 2050 timeframes.

3.1. Discussion of Results

This study utilized the network model Anytown (Walski et al. [9]) to examine the variation in the consumption factor (FQ). The investigation employed a combination of fundamental scenarios, encompassing potential future operating and functional conditions of the network. These scenarios included significant factors such as population growth, climate change, pandemics, fires, and nuanced variations in hourly demand (peak demand).

The Simulated Annealing Heuristic Optimization algorithm, a pivotal element in this assessment, primarily evaluates the likelihood of predefined scenarios, deciphering their probability and ensuring an examination of their probable impact. This aligns with a comprehensive understanding of the dynamics of water consumption within the evolving environmental and demographic conditions in the hypothetical future.

The results obtained from this study show that when using a factor $FQ = 1.0$ in the design combination, the basic scenario occurs when the network is solely tasked with meeting the flow demand. To fulfill this demand, an injection node head of 55 m is required. As a result, the minimum pressure N6 is available at 30.29 m. Additionally, the total flow demanded from the injection tank (with no emitter open) is 658.33 L/s.

The analysis of the scenario G (i.e., $FQ = 1.33$) using the same water level elevation in the injection tank (55 m), shows that by the year 2030, the minimum pressure will occur at node N6 and will have a value of 13.10 m, and by the year 2050, the minimum pressure will be -0.63 m. Additionally, the total flow demanded from the injection tank (with no emitter open) is 875.55 L/s.

For the rest of the proposed combinations and scenarios, the pressures at the nodes are negative, indicating that to meet the future demand considering the proposed combinations here, the system requires a higher head load. See Table 5.

Table 5. Results of scenarios for FQ with injection node head at 55 m.

Combination Identifier	FQ Analysis 2030	Minimum Calculated Pressure 2030 (N6)	FQ Analysis 2050	Minimum Calculated Pressure 2050 (N6)
Basic	1.000	30.29	1.000	30.29
G	1.330	13.10	1.550	−0.63
F	1.640	−6.76	2.339	−64.21
E	1.740	−13.92	2.439	−73.83
D	1.872	−23.91	2.755	−106.41
C	2.172	−48.93	3.055	−140.47
B	$1.872 + Q_F$	−22.47	$2.755 + Q_F$	−101.80
A	$2.172 + Q_F$	−46.45	$3.055 + Q_F$	−134.68

For example, to fulfill the scenario in the year 2030 with Combination A, where $FQ = (2.172 + Q_F)$, an injection load of 128.76 m is necessary for node 13 of the emitter to meet the desired load. This scenario allows the node to operate with a load of 15.00 m, enabling the emitter to contribute 34.86 L/s. Consequently, a total of 130.19 L/s is delivered at node 13. Another result that satisfies Combination A for the year 2050, i.e., $FQ = (3.055 + Q_e)$, requires an injection load of 211 m for node 13 of the emitter to operate at the minimum load, which is a load of 10.33 m, activating the emitter with a flow rate of 28.93 L/s, see Figure 4.

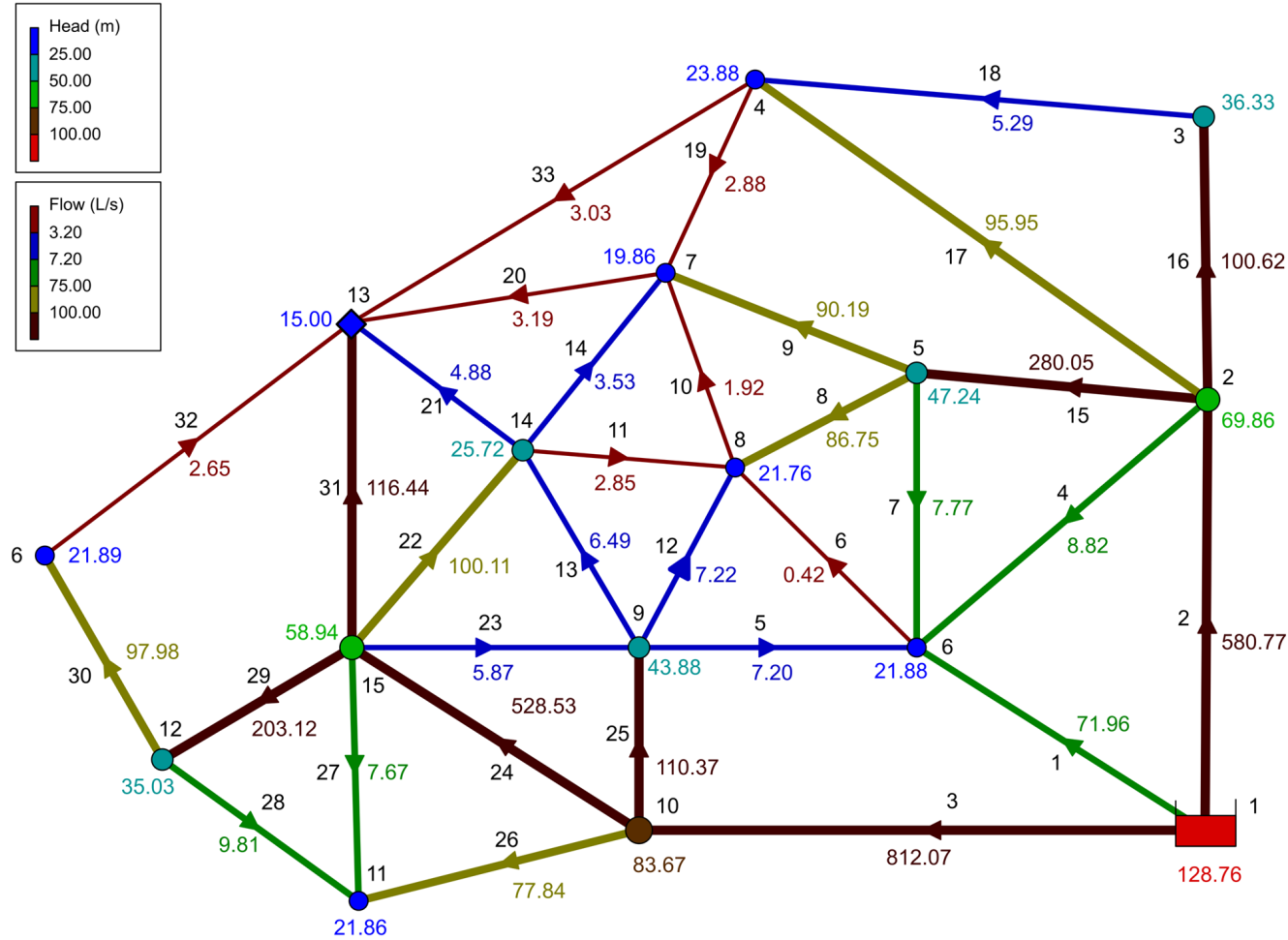


Figure 4. Head and flow distribution of Combination A, Scenario 2030, $2.172 + Q_F$ with emitter flow at node N13.

In Table 6, the Minimum Injection Water Head values in meters, essential to achieve both the desired flow rate and minimum pressure, are presented. Additionally, the Additional Energy Requirement is determined in Kilojoules (kJ) for both scenarios (2030 and 2050) across all seven combinations (denoted as A to G).

Table 6. Minimum Injection Water Head and Energy Requirement Analysis.

Combination Identifier	FQ Analysis 2030	Q (Total) 2030 (L/s)	Minimum Injection Water Head (m)	Additional Energy Requirement (Year 2030) (Kilojoules-kJ)	FQ Analysis 2050	Q (Total) 2050 (L/s)	Minimum Injection Water Head (m)	Additional Energy Requirement (Year 2050) (Kilojoules-kJ)
Basic	1.000	658.33	55.00	0.00	1.000	658.33	55.00	0.00
G	1.330	875.55	56.90	16.32	1.550	1020.45	70.63	156.47
F	1.640	1079.70	76.76	230.48	2.339	1539.90	134.21	1196.58
E	1.740	1145.55	83.92	325.00	2.439	1605.75	143.83	1399.29
D	1.872	1232.40	93.91	470.42	2.755	1813.65	176.41	2160.12
C	2.172	1429.95	118.93	896.80	3.055	2011.20	210.47	3067.40
B	1.872 + Q_F	1261.18	103.78	603.51	2.755 + Q_F	1848.51	185.64	2369.01
A	2.172 + Q_F	1464.81	128.76	1059.92	3.055 + Q_F	2046.06	219.17	3295.20

Notes: Water density used for calculations: 1000 kg/m^3 , resulting in a specific weight of 9.81 N/m^3 based on gravitational acceleration (9.81 m/s^2).

The Minimum Injection Water Heads result in a minimum hydraulic head of 15 m of water column (m) at the critical nodes. Specifically, for the Basic, G, F, E, D, and C combinations, the critical node is identified as (N6). Conversely, for combinations B and A, the critical node is (N13), where the simulated opening of an emitter occurs.

The Additional Energy Requirement (kJ) is calculated by taking the difference between each Minimum Injection Water Head value (m) and the initial reference load height of 55 m. This parameter provides insights into the energy needed to maintain the desired water injection levels.

Finally, it can be inferred that water supply networks designed using conventional technical methods exhibit resilience and functionality withstanding FQ increases up to 50%. However, surpassing this threshold necessitates considerations for applying a higher load to the flow at its head or within hydraulic lines, demanding more energy. Furthermore, the analysis reveals specific energy increment requirements for different scenarios. For instance, in Scenario 2030, Combination A, compared to the Basic Combination, there is a need for an additional energy input of 1059 kJ. Similarly, in Scenario 2050, Combination A, compared to the Basic Combination, the required energy increment amounts to 3295.20 kJ. Figure 4 shows the flow (L/s) results in the lines and Head (m) at the nodes for Combination A, Scenario 2030, ($\text{FQ} \sim 2.172 + Q_F$) with emitter flow at N13.

To attain the required pressure of 15.00 m, referred to as the minimum allowable pressure at the emitter node (N13), a load of at least 128.76 m is required at the injection tank (N1). Figure 5 shows the flow (L/s) results in the lines and pressure (m) at the nodes for Combination A, Scenario 2030, ($\text{FQ} \sim 2.172 + Q_F$) with emitter flow at N13.

For Scenario 2050, Combination A ($3.055 + Q_F$), the lowest pressure is observed at the open emitter node (N13) with a value of 10.33 m. See Table 7 and Figure 6. In contrast, the highest pressure is recorded at node 10, with a value of 128.11 m. A pressure reduction valve should be installed at nodes with service pressures larger than those specified by local regulations. These steps will aid in the optimization of the water distribution system and the efficient supply of water to the network [51].

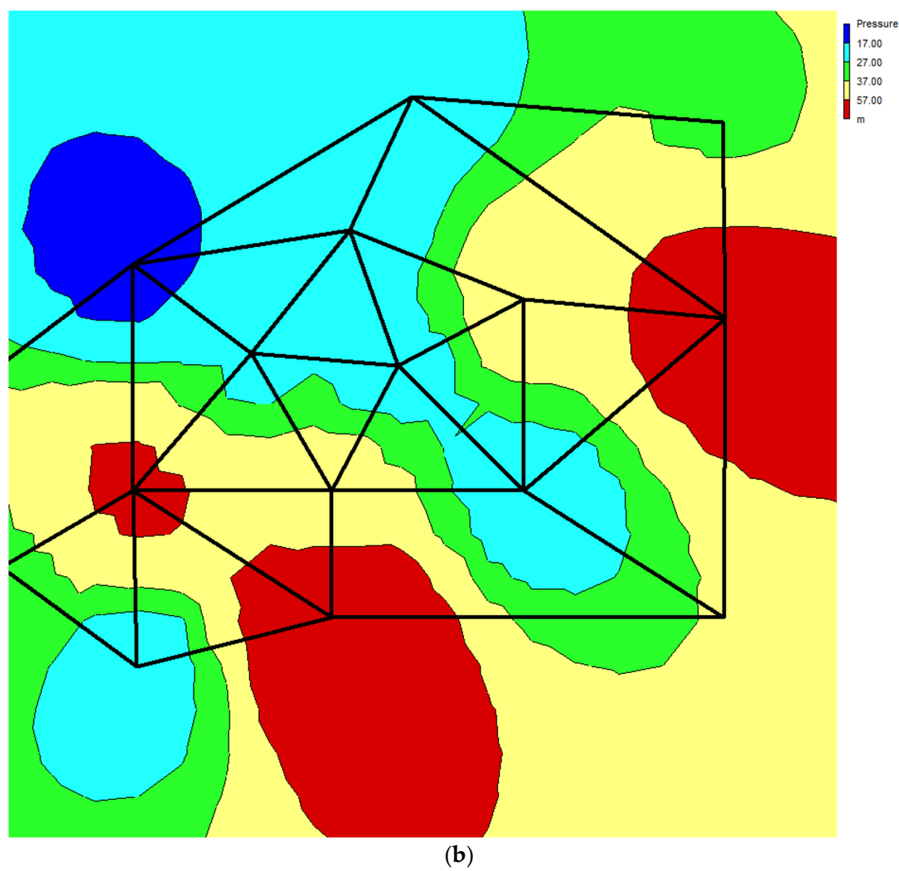
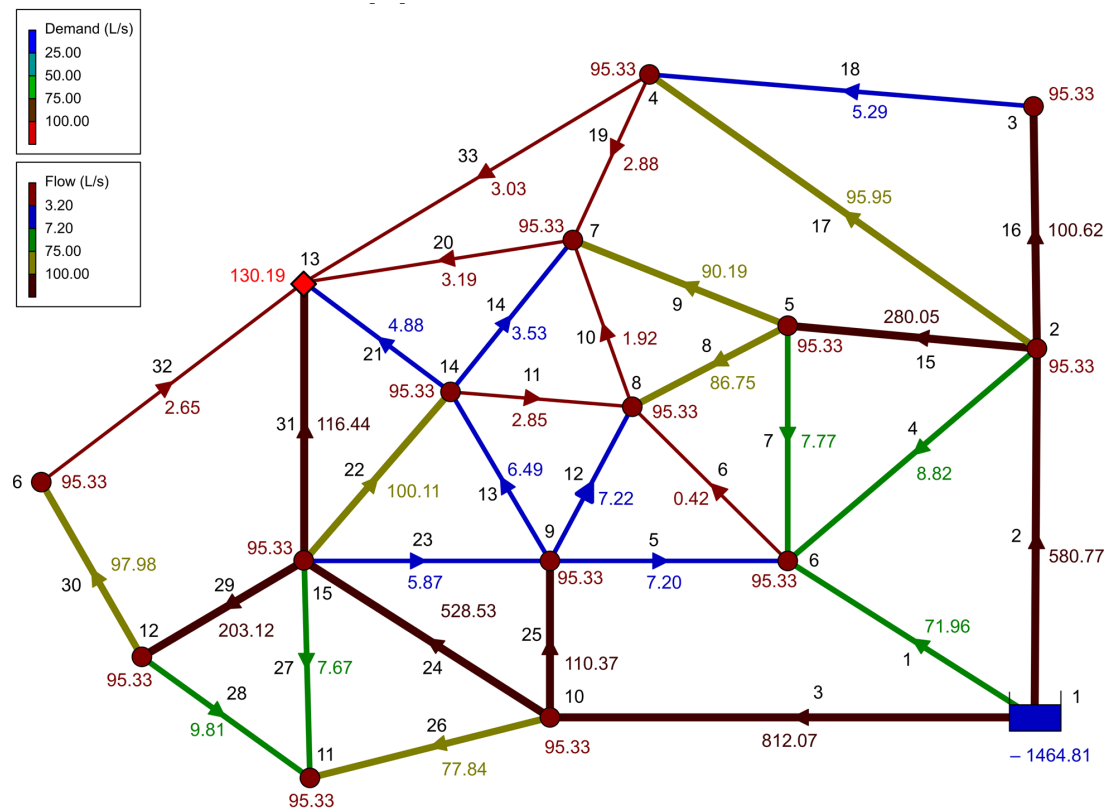


Figure 5. (a) Demand and flow (L/s) distribution for Combination A, Scenario 2030, $2.172 + Q_F$ with emitter flow at node N13. (b) Contour plot–pressure (m) for Combination A, Scenario 2030, $2.172 + Q_F$ with emitter flow at node N13.

Table 7. Results of Modeling for Scenario 2050, Combination A ($3.055 + Q_F$) with Emitter Flow at Node N13: Demands, Pressures, Flow Rates, Pipe Velocities, and Unit Head Losses.

Combination	A	Year: 2050	Injection Height = 211			
$Q_{peak} + Q_{cc} + Q_{cov40} + Q_{PG} + Q_F$			FQ analys: 3.055 + Q_F			
Network Table-Links						
Node ID	Demand L/s	Pressure m	Link ID	Flow L/s	Velocity m/s	Unit Headloss m/Km
Junc 2	134.08	101.60	Pipe 2	811.34	4.13	29.89
Junc 3	134.08	38.77	Pipe 1	100.59	3.20	54.30
Junc 4	134.08	17.06	Pipe 3	1128.19	3.99	22.65
Junc 5	134.08	59.75	Pipe 4	−12.34	1.57	32.61
Junc 6	134.08	12.25	Pipe 5	−10.13	1.29	22.64
Junc 7	134.08	10.41	Pipe 6	−0.11	0.01	0.00
Junc 8	134.08	12.25	Pipe 7	−10.91	1.39	25.96
Junc 9	134.08	53.68	Pipe 8	−121.44	2.47	25.96
Junc 10	134.08	128.11	Pipe 9	123.96	2.53	26.96
Junc 11	134.08	12.63	Pipe 10	1.89	0.24	1.01
Junc 12	134.08	38.53	Pipe 11	−4.51	0.57	5.06
Junc 13	163.01	10.33	Pipe 12	−10.13	1.29	22.64
Junc 14	134.08	21.51	Pipe 13	8.84	1.13	17.58
Junc 15	134.08	83.10	Pipe 14	4.98	0.63	6.07
Junc 16	134.08	14.40	Pipe 15	−390.38	3.11	22.87
Resvr 1	−2040.13	211.00	Pipe 16	141.23	2.88	34.33
P min=	10.33	Junc 13	Pipe 17	133.32	2.72	30.85
			Pipe 18	7.15	0.91	11.87
P max=	128.11	Junc 10	Pipe 19	−3.77	0.48	3.63
			Pipe 20	0.51	0.07	0.04
			Pipe 21	4.99	0.64	6.11
			Pipe 22	−139.72	2.85	33.66
			Pipe 23	8.42	1.07	16.07
			Pipe 24	−730.26	3.72	24.60
			Pipe 25	154.76	3.15	40.67
			Pipe 26	109.09	3.47	63.10
			Pipe 27	−10.85	1.38	25.72
			Pipe 28	−14.14	1.15	14.15
			Pipe 29	−284.29	2.95	24.36
			Pipe 30	136.07	1.93	13.18
			Pipe 31	152.89	3.11	39.77
			Pipe 32	1.99	0.25	1.11
			Pipe 33	−2.61	0.33	1.84

The projected increases in demand from the simulations, encompassing seven combinations and two scenarios in this study, underscore the imperative of injecting more caudal and energy into wastewater distribution networks to meet the imminent surge in global demand and consumption. This aligns with the perspective put forth by Ramos et al. [52], affirming that global water demand is anticipated to persist in its upward trajectory until 2050, reaching 20 to 30% above current levels. This trajectory is chiefly attributed to escalating demands from both industrial and domestic sectors. The findings accentuate the critical need for strategic energy enhancements in water distribution networks, as well as the conservation of water sources, to meet the escalating demands driven by various factors, as explored in this study.

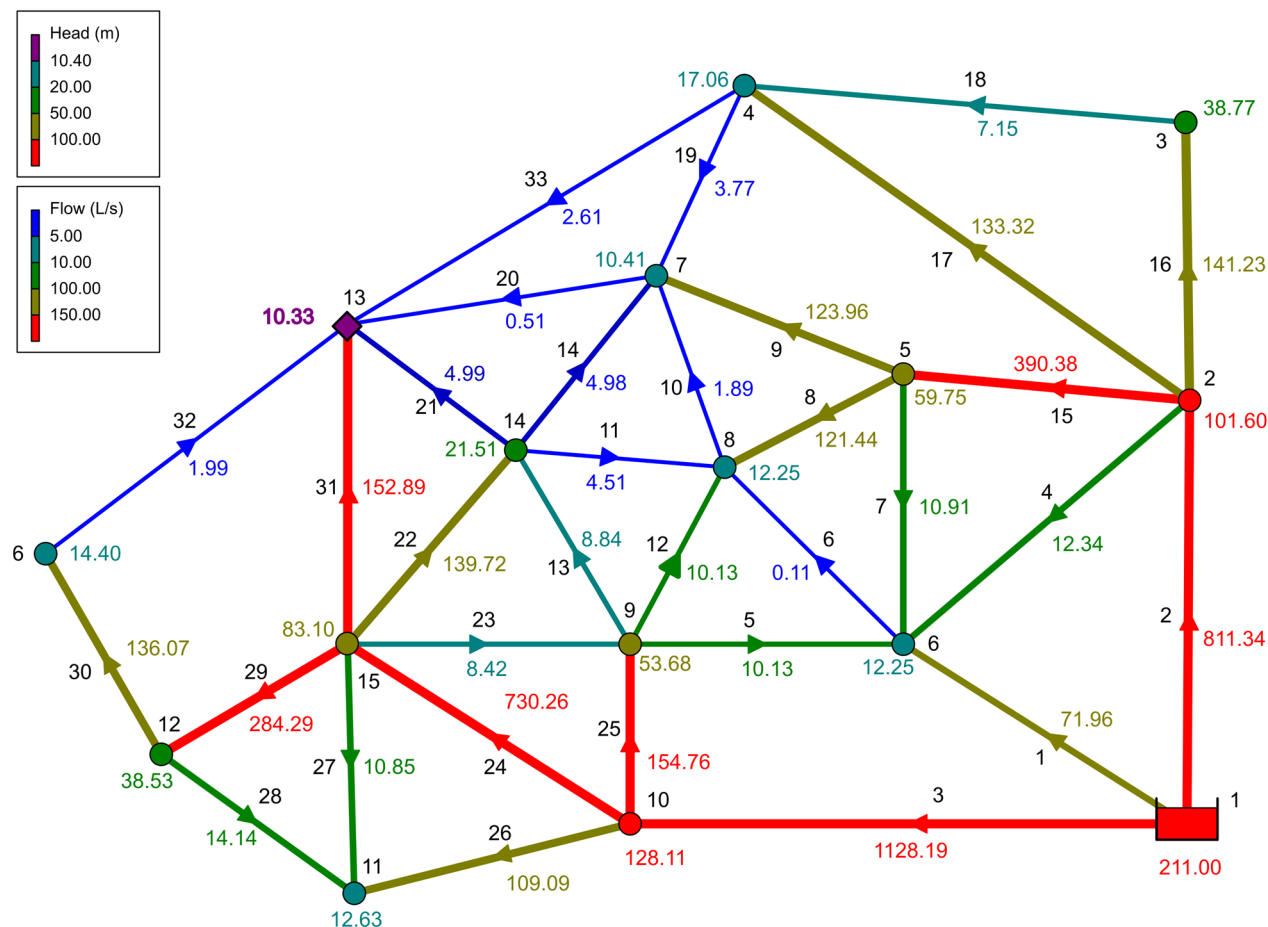


Figure 6. Graphical representation of Scenario 2050, Combination A, with FQ at 231.69%.

3.1.1. Global Influences on Water Consumption Patterns

The discussion on planetary impact phenomena in this study centers on the confluence of escalating domestic water consumption and broader global trends, encompassing rapid population growth, climate change, and pandemics. Although the study does not explicitly explore a specific “planetary theory”, it endeavors to establish correlations among globally impactful factors and their repercussions on water demand.

The inclusion of these phenomena is underscored by their collective influence on water consumption dynamics. Notably, the recent pandemic underscored unique scenarios where peak water consumption coincided with heightened demand due to health-related considerations. Probing into the future, specifically the years 2030 and 2050, the study anticipates additional water demand stemming from climate change and potential fires. The analysis also contemplates a hypothetical future pandemic caused by the patented SARS-CoV-3 [10], projecting an increase in water consumption. While currently deemed improbable, this aligns with the value indicated by Alda-Vidal et al. [11].

3.1.2. Water Efficiency Trends: Motivating Sustainable Reduction in Per-Capita Water Use

This study investigates the correlation between increasing domestic water consumption and global phenomena, such as rapid population growth, climate change, and pandemics affecting distribution networks. It evaluates factors influencing water demand, emphasizing the essential role of water efficiency measures in motivating sustainable reductions in per-capita water use. Recent trends, supported by extensive United States data [53], reveal a consistent decline in per-capita water consumption attributed to advancements in plumbing fixtures and stringent building codes [54]. Integrating these efficiency gains into water demand projections provides a comprehensive perspective on evolving water

usage dynamics, even with population growth. Driving forces encompass technological advancements, the escalating cost of water supply services (or sustainable water service fees), effective environmental regulations, and heightened awareness of water conservation [55].

Richter et al. [56] highlight urban water conservation strategies, emphasizing specific, effective measures. Evaluated cities successfully reduced water usage via a coordinated, multi-strategy approach. Using the San Antonio Water System (SAWS) as a notable case, serving 1.9 million with a dedicated water conservation team of over 20 members, SAWS achieved a remarkable 26% per-capita water use reduction from 1994 to 2018, despite an 85% increase in the service population. In 2018, SAWS reported conserving 4.9 billion liters of water, implementing diverse interventions such as repairing water leaks for low-income customers, transitioning to low-flow toilets, promoting water-conserving practices (e.g., grass removal, irrigation system conversions), and executing public awareness initiatives, including free consultations and personalized home water reports.

Findings underscore the pivotal role of efficient water management practices in achieving sustainable per-capita water use reductions.

3.1.3. Implications for Water Distribution Network Design

It is emphasized that network modeling, typically performed with the maximum hourly factor for technical designs, is essential for understanding the complexity of water consumption patterns. This approach extends beyond conventional considerations based on average daily flows and, at best, maximum hourly flows. The present study demonstrates the importance of exploring various combinations of factors, such as peak consumption demands, hourly variations in demand, and global effects like pandemics, climate change, and potential massive fires, among others, to gain a more comprehensive and future-oriented insight into water demand.

Based on the current modeling and following these findings, it is deemed necessary to conduct a thorough analysis of existing regulations for water distribution network design. This analysis should underpin their evolution, ensuring they are not confined solely to designs based on average daily flows plus fire or, at best, maximum hourly flows. All relevant combinations must be considered in the design, construction, expansion, operation, and maintenance of networks, thereby ensuring a more holistic and resilient approach in future water supply planning.

In technical literature, the maximum water demand is commonly associated with the peak hour. The peak coefficient is calculated by determining the volume of water needed during the peak hour in relation to the average hourly flow demand volume. This is a well-established fact in the field, as normative criteria for water distribution networks serving human consumption typically adhere to sizing based on assumptions made in conventional designs, specifically targeting the “maximum hour” and “maximum day demand + fire” scenarios as indicated by Filion et al. [57].

Saldarriaga and Serna [58] highlight the complexity of the water distribution network design problem, attributing it to the nonlinear relationship between flow and head loss, along with discrete variables such as pipe diameters constrained by market availability. They emphasize the nonlinear connection between the cost function of pipes and their diameters. Their study demonstrates that an optimally cost-effective design aligns with a network demonstrating high reliability during its initial operational phase. However, network reliability gradually diminishes over time, reaching its lowest point during the design period. The authors stress the importance of the Water Distribution Network. WDN operators periodically evaluate network resilience to sustain service reliability [58].

Gonzalez and Saldarriaga [59] focus on optimizing Water Distribution Systems (WDS) for efficient water supply, emphasizing the need for system characterization. They identify key parameters influenced by population density changes via hydraulic gradient, pressure, and specific power analyses. The results show proportional hydraulic gradient changes with demand growth, stable pressure nodes for nearby locations, and consistent energy expenditure relative to the percent difference.

According to Filion et al. [57], low-pressure failures in low-demand months are linked to demand fluctuations at high-use nodes. Anticipating annual damages in design helps balance costs and damages. The study suggests a multi-objective design considering cost efficiency and enhanced system capacity to address diverse demand patterns causing hydraulic failures in water networks.

Based on the study findings, it is pertinent to recommend a review for updating existing regulations. Coordinated strategies involving national, regional, and local policymakers are fundamental to mitigating the impact of global phenomena on water supply systems. A comprehensive approach, integrating active physical network management, is necessary to address the consequences of climate change, population growth, pandemics, and future water management.

The findings of this study extend even further than those proposed by Balacco et al. [60]. Their analysis, focused on the behavior of peak flow factors derived from available time series, asserts a greater uniformity in daily water consumption over the past fifty years. They rationalize relatively low maximum coefficient values and emphasize the limited representativeness of certain expressions found in the literature, often recommended by technical manuals, indicating the potential for unnecessary oversizing of urban water network supplies. It is worth noting that their analysis does not include extreme phenomena that could lead to an increase in demand, which are increasingly possible, although their occurrence is neither anticipated nor desired.

Coordinated strategies should be used by national, regional, and local policymakers and planners to mitigate the effects of global phenomena on water supply systems. Along with active physical network management, a comprehensive strategy is required to address the consequences of climate change, population increase, pandemics, and water management.

It is becoming more and more important to ensure that there is enough water for the population, so steps must be taken from the design stage via operation and maintenance, and now, more justifiably, rehabilitation and expansion phases, as appropriate in each case, to ensure that this precious resource is conserved and distributed fairly to all users.

3.1.4. Water Infrastructure Optimization

In the pursuit of optimizing water infrastructure, a thorough evaluation of the existing pipe network is recommended. This involves identifying pipes that require cleaning and lining via a detailed inspection of structural integrity, corrosion levels, and pressure-affecting deposits [61]. Determining desired pressure levels at various network points is fundamental for efficient water supply, and hydraulic modeling software should be employed to optimize the system layout, enhancing pressure distribution [62]. A cost analysis should be performed, encompassing expenses related to new installations, cleaning and lining of existing pipes, and material choices for durability and corrosion resistance [63]. The utilization of optimization algorithms aims to find a recommended cost-effective balance between new components and maintenance requirements for existing pipes [64]. Environmental impact considerations should prioritize sustainable options in material selection and construction practices [65]. Ensuring compliance with relevant regulations and standards is recommended in the selection of components and maintenance activities. Additionally, a comprehensive risk assessment is recommended to cover long-term maintenance needs, demand uncertainties, and the lifespan of diverse materials, particularly considering unconventional yet potentially impactful demands on the network.

3.2. Limitations

The recommended models and approaches may have inherent limitations and may not be appropriate for all real-world settings. The study focuses on specific factors and may not cover all of the potential implications on water use and distribution. These limitations should be considered when interpreting the findings.

Despite these limitations, this work is important because it sheds light on the issues of water demand estimation and distribution planning. The findings contribute to a better knowledge of the elements that influence water demand and supply, allowing for more informed decision-making in the efficient management of water resources. This study, by addressing the urgency of sustainable water management, provides a path to improve water system resilience and helps the creation of effective plans for future water demand projections and conservation measures.

4. Conclusions

Innovative and revolutionary ideas must be used in order to build a sustainable future and handle the difficulties brought on by growing demand and significant changes in the availability of water. This study focused on estimating increases in water consumption for the years 2030 and 2050 while taking into account planetary impact events such as population expansion, climate change, and pandemics.

By creating a network model, it was possible to investigate how the water supply system's consumption factor (FQ) may change under several probable future scenarios. The results showed that to fulfill the anticipated future home water demands, there would be large increases in the energy needed. Moving beyond conventional management techniques, adaptive approaches and continuous dynamics must be adopted to achieve water conservation and sustainable water management.

In this study, a water consumption projection was analyzed, combining possible global scenarios for the years 2030 and 2050 using the method of fundamental scenario combination. The adapted simulated annealing algorithm was applied to the consumption projection.

Author Contributions: Conceptualization, H.M.B.-M., M.L.-P., F.J.M.-S., M.Q.-C. and S.Q.-C.; Data curation, M.L.-P., M.Q.-C. and S.Q.-C.; Methodology, H.M.B.-M., M.Q.-C. and S.Q.-C.; Validation, H.M.B.-M. and F.J.M.-S.; Writing—original draft, H.M.B.-M.; Writing—review and editing, F.J.M.-S. All authors have read and agreed to the published version of the manuscript.

Funding: The authors express their deep gratitude to the Universidad Técnica Particular de Loja (UTPL, RUC: 1190068729001, St. Marcelino Champagnat, San Cayetano Alto) for funding the present research work.

Data Availability Statement: The data presented in this study are available on request from the corresponding author.

Conflicts of Interest: The authors declare no conflicts of interest.

Appendix A. Mathematical Details of the Water Consumption Projection Model

The water consumption projection model, as explained in the main text, is formulated using the closed Newton–Cotes integration equation with order $n = 1$. This mathematical approach is designed to forecast future water consumption considering the initial consumption, the targeted annual percentage increase, and the cumulative impact of global temperature changes over time. See Equation (2).

The integral of the global temperature function from 2000 to t represents the cumulative change in temperature over time. This equation captures the cumulative impact of incremental changes in global temperature, accumulating the net change throughout the modeled time period. The maximum value of the model is reached when t equals 2060.

The model employs a multiplicative structure, relating variables via multiplication among the main terms, each influencing the result proportionally.

It involves mathematical functions of the dependent variables Q and T in terms of the independent parameter time (t) in years and the projected global temperature variation.

The model also involves historical annual data on temperature change worldwide, from the year 1880 and projected to 2060.

It originates from the analysis of temporal data on temperature variation and projections estimated by the authors Noll, [66]; National Geographic, [67]; and Vidal, [68].

Additionally, the temporal derivatives in ΔT and the integral of $T(y)$ impart an approximate differential character. See Figure A1.

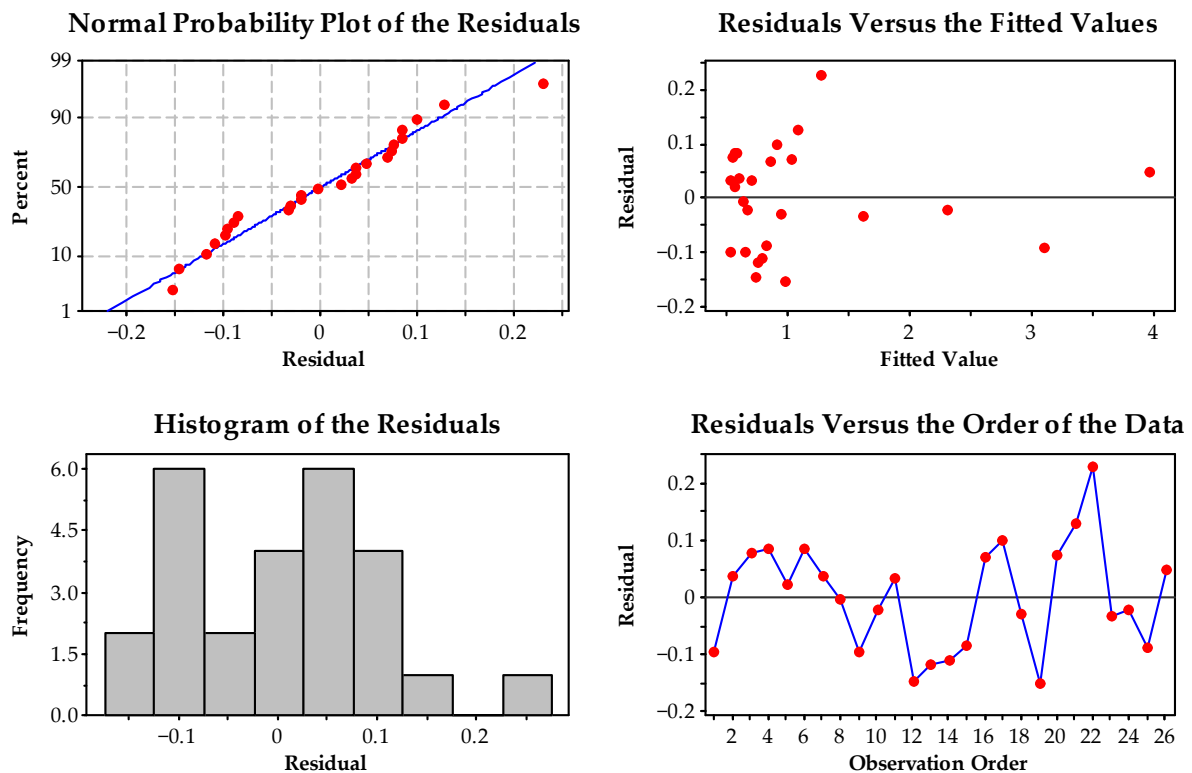


Figure A1. The residuals (difference between observed and fitted values). In the Normal Probability Plot of the Residuals, the red points represent the standardized residuals plotted against their corresponding percentiles on the y-axis, while the blue line depicts the expected trend if the residuals follow a normal distribution. Deviations of the red points from the blue line suggest departures from normality in the residuals. Conversely, in the Residuals Versus Order of the Data, the red dots represent the residuals plotted against the order of the data on the x-axis, while the blue line simply connects these points, illustrating the trajectory of each residual (x, y), where x represents the observation order and y represents the residual value.

The residual plot, Figure A1, shows the residuals (difference between observed and fitted values) scattered randomly around the horizontal axis with no discernible pattern. This suggests that the linear model fits the data reasonably well, with no systematic lack of fit. The variability of the residuals seems fairly constant over the range of fitted values, indicating that the assumption of equal variance is satisfied.

Computation of the annual temperature integral ($\int dT(y)$) via 40-year (2020 to 2060) cumulative sums to represent the cumulative effect was employed. The best-fitting model with the highest R-squared value was determined via cubic regression analysis between year-to-year variations in Q and predictors ΔT and $\int dT(y)$.

The adjusted model minimizing autocorrelated residuals and maximizing predictive R-squared was formulated; see Equation (A1).

$$\frac{dT}{dy} = \frac{(-70.29 + 0.06792 \cdot y - 0.000015 \cdot y^2)}{\beta_i} \quad (\text{A1})$$

Rewriting the equation in integrated form yields Equation (A2), applicable for $t_1 = 2000$ and $t_2 = 2060$.

$$\int_{t_1}^{t_2} dT = \int_{2000}^{2060} \left(\frac{(-70.29 + 0.06792 \cdot y - 0.000015 \cdot y^2)}{\beta_i} \right) dy \quad (\text{A2})$$

In the modeling process, the constant of integration (C) is determined by optimizing the model parameters to best fit the available year-versus-temperature increment data. This optimization process incorporates C as an integral part of refining the model, aiming to find its optimal value and improve alignment with observed data. Specifically, for this model, the resulting C value is 48,431. See Equation (A3) and Figure A2.

$$T(y) = \left[-\frac{70.29 \cdot y}{\beta_i} + \frac{0.06792 \cdot y^2}{2 \beta_i} - \frac{0.000015 \cdot y^3}{3 \beta_i} + C \right]_{2000}^{2060}$$

$$T(y) = \left[-\frac{70.29 \cdot y}{\beta_i} + \frac{0.06792 \cdot y^2}{2 \beta_i} - \frac{0.000015 \cdot y^3}{3 \beta_i} + 48,431 \right]_{2000}^{2060} \quad (\text{A3})$$

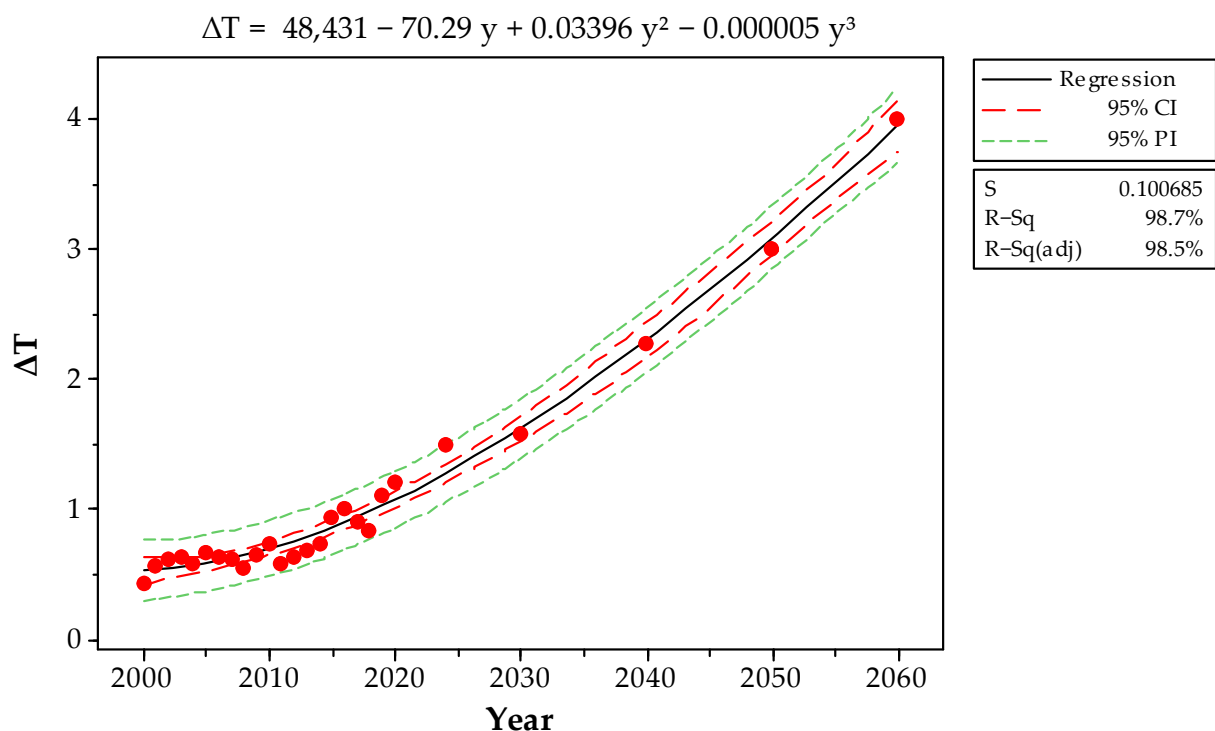


Figure A2. The fitted line plot, regression ΔT .

The fitted line plot (Figure A2) depicts the estimated linear regression line overlaid on a scatter plot of the observed data. The line bisects the data point cluster, confirming that the linear model successfully captures the predominant trend within the data. The evenly dispersed residuals, as evidenced by the uniform spread of points above and below the line, reaffirm that the linear model provides an adequate fit without any major systematic discrepancies. Moreover, the R-squared statistic of 0.987 signifies that the linear model elucidates 98.7% of the variance in the response after controlling for the mean. This elevated R-squared score offers additional validation of an exceptionally robust linear association linking the explanatory and outcome variables under examination. Both the graphical and numerical diagnostic measures endorse the aptness of the fitted linear model for representing the relationship embodied in the source data (Year vs. ΔT).

Table A1 provides insights into the values of the Increase in Consumption Factor ($FQ = (1 + \Delta T/100) (1 + \int T(y)dy)$), corresponding to the sum of the Q_{peak} factor and Q_{CC} . It outlines the denominator factors for $T(y)$ in the years 2030 and 2050 across different combinations labeled A, B, C, D, and E. Each scenario for both 2030 and 2050 is represented in columns that include the combination identifier, the denominator factor for $T(y)$ in 2030 (β_{2030}), the corresponding factor for 2050 (β_{2050}), and the discharge factor for each respective year.

Table A1. Values of the Increase in Consumption Factor FQ .

Combination	Denominator Factor for $T(s)$ for 2030 (β_{2030})	$\int T(y) dy$	$(1 + \frac{\Delta T}{100}) (1 + \int_0^t T(s) ds)$ Factor to the Year 2030	Denominator Factor for $T(s)$ for 2050 (β_{2050})	$\int T(y) dy$	$(1 + \frac{\Delta T}{100}) (1 + \int_0^t T(s) ds)$ Factor to the Year 2050
A	530.7973	0.320139	1.33000	534.09613	0.536935	1.55000
B	270.6562	0.627841	1.64000	217.37157	1.319285	2.33900
C	233.7081	0.727099	1.74000	202.17607	1.418442	2.43900
D	198.1211	0.857703	1.87158	165.61564	1.731570	2.75479
E	147.0637	1.155479	2.17158	141.33525	2.029041	3.05479

Notes: To compute the discharge factors ($FQ = (1 + \frac{\Delta T}{100}) (1 + \int_0^t T(y) dy)$) for the years 2030 and 2050, the values of $\Delta T/100$ are taken into account, with $\Delta T/100$ (2030) = 0.0075 and $\Delta T/100$ (2050) = 0.0085.

Appendix B. Modeling Water Demand Growth as a Product of Population and per Capita Consumption Trends

The $Q_{PG}(y)$ model aims to estimate future water demand by accounting for projected population growth trends and per capita consumption patterns over time. The mathematical formulation draws on recent population growth forecasts (Philips et al. [69], Romero et al. [70]) and historical municipal water consumption data.

Specifically, population dynamics were encapsulated in the derivative $P'(y)$ the rate of population change per year was obtained. See Equation (A4).

$$\frac{dP}{dy} = \frac{(-0.7662 \cdot y + 1621)}{\beta_p^{\varnothing_p}} \quad (A4)$$

Integrating $P'(y)$ yielded $\int P'(y)dy$, describing total population size as a function of time. See Equation (A5).

$$\int_{t_1}^{t_2} dP = \int_{1990}^{2100} \left(\frac{(-0.7662 \cdot y + 1621)}{\beta_p^{\varnothing_p}} \right) dy \quad (A5)$$

In the model refinement, determining the constant of integration (C) involves a detailed approach. This process incorporates specific mathematical parameters tailored to the inherent characteristics of the dataset. See Equation (A6).

$$P(y) = \left[\frac{1621 \cdot y}{\beta_p^{\varnothing_p}} + \frac{0.7662 \cdot y^2}{2 \beta_p^{\varnothing_p}} + C \right]_{1990}^{2100}$$

$$P(y) = \left[\frac{1621 \cdot y}{\beta_p^{\varnothing_p}} + \frac{0.7662 \cdot y^2}{2 \beta_p^{\varnothing_p}} - \frac{1,703,526}{\beta_p^{\varnothing_p}} \right]_{1990}^{2100} \quad (A6)$$

The value of C, calculated as $C = [-1,703,526/(\beta_p^{\varnothing_p})]$, results from the interplay of parameters $\beta_p = 202.14$ and $\varnothing_p = 1.7760$. This formulation ensures integration, attuned to the dynamic characteristics encapsulated within the model. Refer to Equation (A6) and Figure A3.

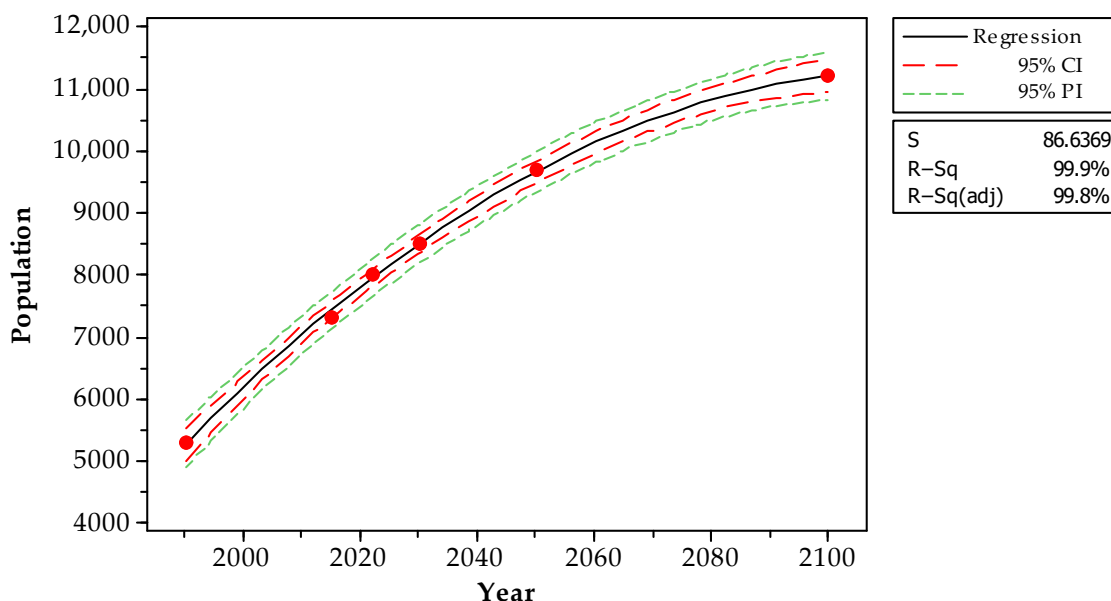


Figure A3. The fitted line plot: regression analysis of annual population growth rate.

This fitted line plot, Figure A3, shows the original average consumption data points (for the 18 cities over time) along with the fitted linear regression line. The R-squared value is 46.9%, indicating a moderate linear relationship between the variables. Though not an extremely tight fit, given that this model incorporates data across 18 cities spanning over 20 years, capturing the general increasing trend is reasonable. There may be additional factors influencing each city's consumption from year to year that introduce some variability around the trend. However, with a diverse sample of cities, there are likely common macro factors that lend themselves to an overall linear modeled trend. The residuals exhibit constant variance and no systematic patterns, supporting the use of this aggregate linear model across cities despite the R-squared value not being exceptionally high. Justifying the use of this model with a larger sample of cities covering a long time period may provide more reliable and meaningful insights than finding tighter-fitting models of individual cities with more limited data.

The residual plot in Figure A4 illustrates the relationship between residuals (depicted on the vertical axis) and fitted values (depicted on the horizontal axis) within the context of a linear regression model that has been applied to analyze the average water consumption data across 18 cities over time. See Figure A4.

The residuals in Figure A4 appear to be randomly scattered around zero with no apparent patterns or trends, indicating that a linear model is appropriate.

The polynomial regression yielded an equation modeling population as a quadratic function of time, with both linear and quadratic terms proving to be highly statistically significant (F test p -values < 0.01). The overall model fit was extremely strong, with an R-squared of 99.9% and an adjusted R-squared of 99.8%, meaning over 99% of the variance in the historical population is captured by the quadratic trend.

The goodness of fit and significance testing indicates this quadratic regression model accurately reflects the nonlinear accelerating population growth trajectory over the study period [69,70]. The precision of the equation in modeling historical data lends credibility for extrapolating future projections. The derived functional form establishes a robust foundation for integration into the integrated water demand model via Equation (A6).

The F-test values, along with negligible p -values, provide overwhelming evidence to reject the null hypothesis of no relationship in favor of this robust quadratic linkage between year and population size. Furthermore, the additional predictive capability of the quadratic term over just a linear trend is supported by its high F score of 181.37 and highly significant p -value of 0.001.

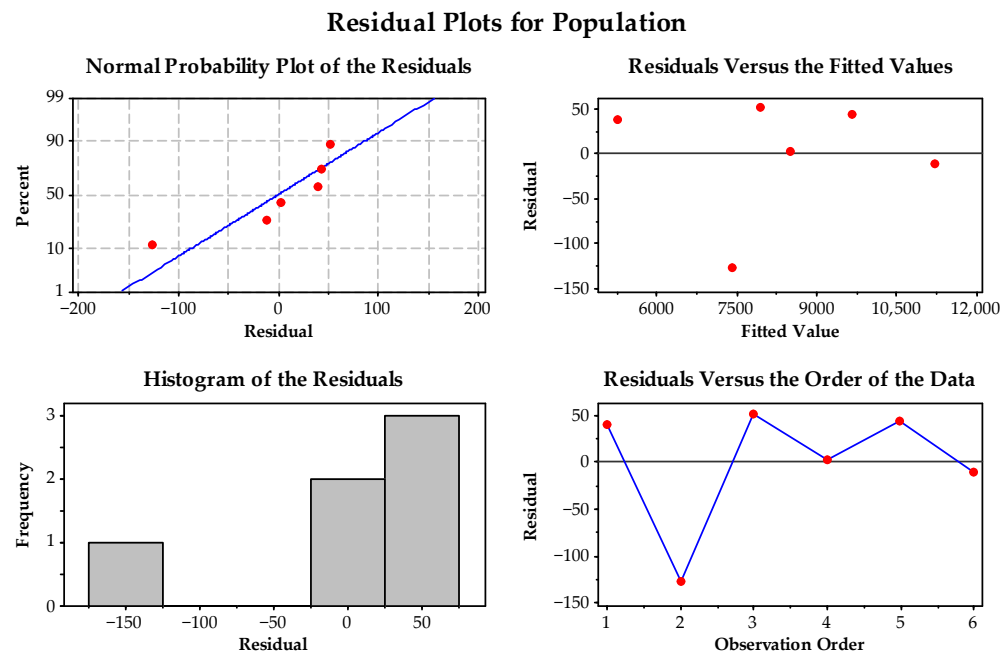


Figure A4. Residual plots for regression analysis of annual population growth rate. Refer to the explanation provided in Figure A1 for details regarding the red dots and blue lines.

Likewise, per capita water consumption patterns were modeled using the function $C(y)$, derived from the consumption statistics of the 18 cities in the IBNET database [71]—the only cities with publicly available annual municipal water data from 2000–2020. See Equation (A7).

$$\frac{dC}{dy} = \frac{0.7383}{\beta_c^{\varnothing_c}} \quad (\text{A7})$$

Taking the derivative $C'(y)$ gave the rate of per capita consumption change over time. See Equation (A8).

$$\int_{t_1}^{t_2} dC = \int_{2000}^{2100} \left(\frac{0.7383}{\beta_c^{\varnothing_c}} \right) dy \quad (\text{A8})$$

Integrating this function, $\int C'(y)dy$, quantified total per capita consumption. In a parallel manner to the determination of the integration constant C , the refinement of the model involves the calculation of another integration constant, denoted as K , for the per capita water consumption patterns. This process employs a similarly detailed approach, incorporating specific mathematical parameters tailored to the dataset's intrinsic characteristics. See Equation (A9).

$$C(y) = \left[\frac{0.7383 \cdot y}{\beta_c^{\varnothing_c}} + K \right]_{2000}^{2100}$$

$$C(y) = \left[\frac{0.7383 \cdot y}{\beta_c^{\varnothing_c}} - \frac{1370}{\beta_c^{\varnothing_c}} - \mu \right]_{2000}^{2100} \quad (\text{A9})$$

The function $C(y)$, derived from consumption statistics of the 18 cities in the IBNET database [71], is expressed as $C(y) = [(((−1370 + 0.7383 \times y) - (−1370 + 0.7383 \times y_{2000}))/\beta_c^{\varnothing_c}) - \mu]$, where y represents the year. The integration constant for this function is defined as $K = [(-1370/\beta_c^{\varnothing_c}) - \mu]$. The derived integration constant values that ensure the model's satisfaction are as follows: $\beta_c = 96.2969$; $\varnothing_c = 0.79675$; $\mu = 0.0763283$. This formulation ensures a thorough integration, finely tailored to the dynamic characteristics within the model. Refer to Equation (A9) and Figure A5.

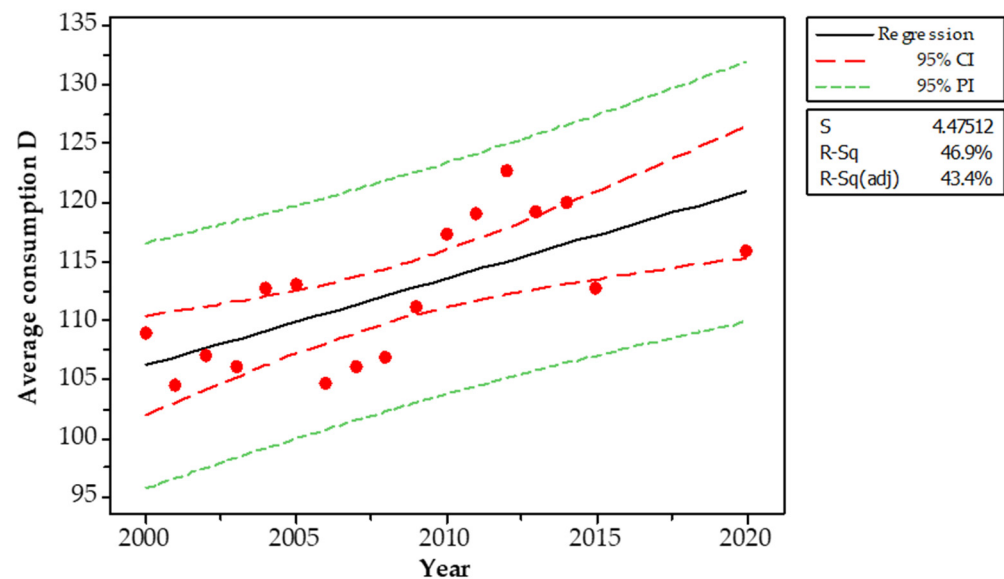


Figure A5. Fitted line plot: regression analysis of annual consumption growth rate.

This fitted line plot shows the original average consumption data points (for the 18 cities over time [71]) along with the fitted linear regression line. The R-squared value is 46.9%, indicating a moderate linear relationship between the variables. Though not an extremely tight fit, given that this model incorporates data across 18 cities spanning over 20 years, capturing the general increasing trend is reasonable. There may be additional factors influencing each city's consumption from year to year that introduce some variability around the trend. However, with a diverse sample of cities, there are likely common macro factors that lend themselves to an overall linear modeled trend. The residuals exhibit constant variance and no systematic patterns, supporting the use of this aggregate linear model across cities despite the R-squared value not being exceptionally high. Justifying the use of this model with a larger sample of cities covering a long time period may provide more reliable and meaningful insights than finding tighter-fitting models of individual cities with more limited data.

The residual plot in Figure A6 illustrates the relationship between residuals (depicted on the vertical axis) and fitted values (depicted on the horizontal axis) within the context of a linear regression model that has been applied to analyze the average water consumption data across 18 cities over time [71]. The residuals appear to be randomly scattered around zero with no apparent patterns or trends, indicating that a linear model is appropriate. The variance of residuals seems relatively constant across fitted values, meeting the assumption of homoscedasticity as a statistical condition for regression analysis, which refers to the equality of variances of errors across all levels of the independent predictor variable. There are no extreme outlier residuals. Overall, this residual plot supports using the linear regression on this dataset with 18 cities.

Multiplying the two integrals combines projected population growth and per capita use to estimate future aggregate municipal water demand, $Q_{PG}(y)$. Equation (A10) shows the mathematical developments of $P(y)$, $C(y)$, and the specifics of the $Q_{PG}(y)$ integral formulation. See Equation (3).

$$Q_{PG}(y) = \int_{1990}^{2100} (P'(y) dy) \cdot \int_{2000}^{2100} (C'(y) dy) \quad (\text{A10})$$

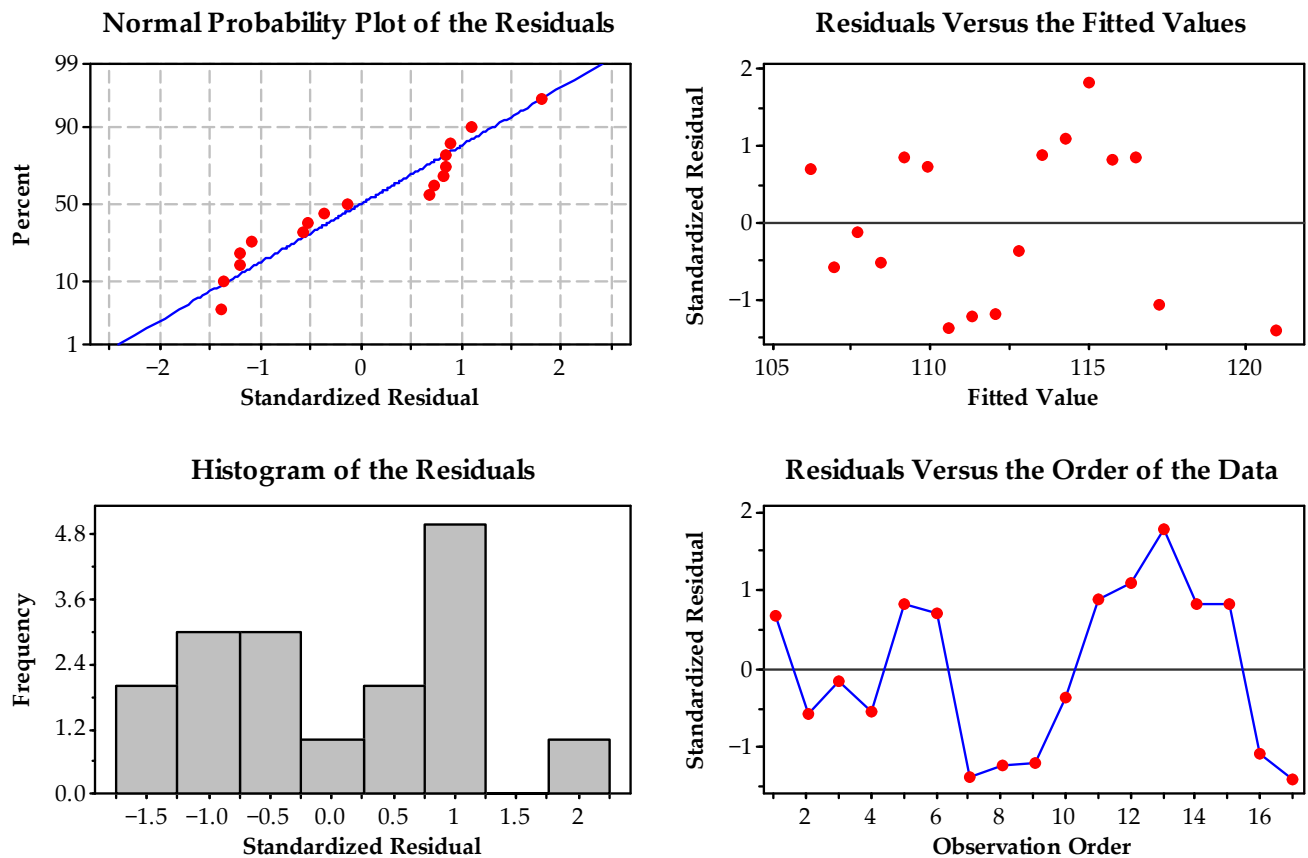


Figure A6. Residual plots for regression analysis of average consumption growth rate. Refer to Figure A1 for details.

Table A2 displays parameter fitting data related to Population, $P(t)$, and Consumption $C(t)$ by year and product for water demand projection. The highlighted years in this study are systematically identified, with corresponding values for population determined accordingly. The results for each year of $\int P'(y)dy$ and $\int C'(y)dy$ are presented in separate columns. The final column showcases the product of these integrals, generating the coefficient $Q_{PG}(y)$.

Table A2. Parameter fitting data: Population, $P(t)$, and $C(t)$ by year and product for projecting water demand.

Year	Population	$\int P'(y)$	$\int C'(y)$	$\int P'(y) \times \int C'(y)$
1990	5300	0.0000	−0.2703	
2015	7300	0.1742	0.2147	0.037
2022	8000	0.2161	0.3505	0.076
2030	8500	0.2602	0.5056	0.132
2050	9700	0.3534	0.8936	0.316
2100	11,200	0.4785	1.8636	0.892

Notes: Notably, the values for both the years 2030 and 2050 are highlighted in the final column, offering insights into the water demand projection for the specified time frames in the analysis conducted for this study, as presented in Table 1.

As a concluding remark for the explanatory appendix, it is essential to recognize numerous avenues for future research. Notable contributions, such as Zhou's [72] work, underscore the ongoing necessity for advancements in forecasting. Studies focused on predicting daily water consumption could utilize a time series model with equations for trend, seasonality, climatic correlation, autocorrelation, and persistence components.

The continuous exploration of advanced predictive models is vital for refining future consumption estimations, facilitating timely anticipation, and addressing extreme demands. As emphasized by Haque et al. [73] and El-Rawy et al. [74], predicting the potential impacts of climatic changes on water demand is essential for implementing measures to mitigate adverse effects on water supply. This ensures that demand is met whenever and wherever required, enhancing the accuracy of future consumption estimations and enabling decision makers to anticipate and address extreme demands in a timely manner.

References

1. Data Commons 2024, Place Explorer. Demographics, Data Commons. Available online: <https://datacommons.org/place/Earth?category=Demographics> (accessed on 3 March 2024).
2. Population Division, Department of Economic and Social Affairs, United Nations. *World Population Prospects: The 2012 Revision, Key Findings and Advance Tables*; Working Paper No. ESA/P/WP.227; Population Division, Department of Economic and Social Affairs, United Nations: New York, NY, USA, 2013.
3. UN Water. *Water for a Sustainable World. Data and Figures. United Nations Report on World Water Resources. United Nations Educational, Scientific and Cultural Organization. World Water Assessment Programme*; UN Water: Geneva, Switzerland, 2015.
4. UN Water. *UN-Water Policy Report on Climate Change and Water. SWEDEN. Swiss Agency for Development and Cooperation SDC. Ministry of Foreign Affairs of the Netherlands*; UN Water: Geneva, Switzerland, 2019.
5. UN. *Climate Change and Water. UN-Water Policy Brief. Coordinated by the UN-Water Expert Group on Water and Climate Change*; UN: Geneva, Switzerland, 2019.
6. Zubaidi, S.L.; Ortega-Martorell, S.; Al-Bugharbee, H.; Olier, I.; Hashim, K.S.; Gharghan, S.K.; Kot, P.; Al-Khaddar, R. Urban Water Demand Prediction for a City that Suffers from Climate Change and Population Growth: Gauteng Province Case Study. *Water* **2020**, *12*, 1885. [CrossRef]
7. UNDP. Goal 6: Clean Water and Sanitation. Sustainable Development Goals. 2020. Available online: <https://www.undp.org/sustainable-development-goals/clean-water-and-sanitation> (accessed on 10 January 2024).
8. UN Water. UN 2023 Water Conference: Water Action Agenda. In Proceedings of the UN 2023 Water Conference, New York, NY, USA, 22–24 March 2023.
9. Walski, T.M.; Brill, E.D., Jr.; Gessler, J.; Goulter, I.C.; Jeppson, R.M.; Lansey, K.; Lee, H.-L.; Liebman, J.C.; Mays, L.; Morgan, D.R.; et al. Battle of the network models: Epilogue. *J. Water Resour. Plan. Manag.* **1987**, *113*, 191–203. [CrossRef]
10. Sillekens, P.T.G. Nucleic Acid Sequences That Can Be Used as Primers and Probes in the Amplification and Detection of SARS Coronavirus. SARS-CoV-3. International Publication Number: WO 2004/111274 A1, 23 December 2004. International Application Published Under the Patent Cooperation Treaty (PCT). Available online: <https://patentimages.storage.googleapis.com/7b/4c/4c/230b8e35ca55ac/WO2004111274A1.pdf> (accessed on 28 January 2023).
11. Alda-Vidal, C.; Smith, R.; Lawson, R.; Browne, A.L. *Understanding Changes in Household Water Consumption Associated with COVID-19*; Artesia Consulting: Yate, UK, 2020.
12. Kim, D.; Yim, T.; Lee, J.Y. Analytical study on changes in domestic hot water use caused by COVID-19 pandemic. *Energy* **2021**, *231*, 120915. [CrossRef] [PubMed]
13. Jia, X.; Shahzad, K.; Klemeš, J.J.; Jia, X. Changes in water use and wastewater generation influenced by the COVID-19 pandemic: A case study of China. *J. Environ. Manag.* **2022**, *314*, 115024. [CrossRef] [PubMed]
14. Kazak, J.K.; Szwedrowski, S.; Pilawka, T.; Tokarczyk-Dorociak, K.; Janiak, K.; Swiader, M. Changes in water demand patterns in a European city due to restrictions caused by the COVID-19 pandemic. *Desalination Water Treat.* **2021**, *222*, 1–15. [CrossRef]
15. Sowby, R.B.; Lunstad, N.T. Considerations for studying the impacts of COVID-19 and other complex hazards on drinking water systems. *J. Infrastruct. Syst.* **2021**, *27*, 02521002. [CrossRef]
16. Zechman Berglund, E.; Thelemaque, N.; Spearing, L.; Faust, K.M.; Kaminsky, J.; Sela, L.; Kadinski, L. Water and Wastewater Systems and Utilities: Challenges and Opportunities During the COVID-19 Pandemic. *J. Water Resour. Plann. Manag.* **2021**, *147*, 02521001. [CrossRef]
17. Sowby, R.B.; Hansen, C.H. Short-Term and Sustained Redistribution of Residential and Non-residential Water Demand due to COVID-19. *Authorea* **2023**, preprints.
18. Li, D.; Engel, R.A.; Ma, X.; Porse, E.; Kaplan, J.D.; Margulis, S.A.; Lettenmaier, D.P. Stay-at-Home Orders during the COVID-19 pandemic reduced Urban Water use. *Environ. Sci. Technol. Lett.* **2021**, *8*, 431–436. [CrossRef]
19. Lüdtke, D.U.; Luetkemeier, R.; Schneemann, M.; Liehr, S. Increase in daily household water demand during the first wave of the COVID-19 pandemic in Germany. *Water* **2021**, *13*, 260. [CrossRef]
20. Balacco, G.; Totaro, V.; Iacobellis, V.; Manni, A.; Spagnoletta, M.; Piccinni, A.F. Influence of COVID-19 spread on water drinking demand: The case of Puglia Region (Southern Italy). *Sustainability* **2020**, *12*, 5919. [CrossRef]
21. Spearing, L.A.; Thelemaque, N.; Kaminsky, J.A.; Katz, L.E.; Kinney, K.A.; Kirisits, M.J.; Faust, K.M. Implications of social distancing policies on drinking water infrastructure: An overview of the challenges to and responses of US utilities during the COVID-19 pandemic. *ACS ES&T Water* **2020**, *1*, 888–899.

22. World Water Development Report (WWDR). Global Water Resources under Increasing Pressure from Rapidly Growing Demands and Climate Change, according to New UN World Water Development Report. United Nations World Water Assessment Programme. 2012. Available online: https://www.jkgeography.com/uploads/1/0/8/4/108433405/pressures_on_water_supples_unesco.pdf (accessed on 16 October 2023).
23. Buchberger, S.G.; Wu, L. Model for instantaneous residential water demands. *J. Hydraul. Eng.* **1995**, *121*, 232–246. [\[CrossRef\]](#)
24. Martínez-Solano, J.; Iglesias-Rey, P.L.; Pérez-García, R.; López-Jiménez, P.A. Hydraulic analysis of peak demand in looped water distribution networks. *J. Water Resour. Plan. Manag.* **2008**, *134*, 504–510. [\[CrossRef\]](#)
25. Jones, V.; Whitehouse, S.; McEwen, L.; Williams, S.; Gorell Barnes, L. Promoting water efficiency and hydrocitizenship in young people's learning about drought risk in a temperate maritime country. *Water* **2021**, *13*, 2599. [\[CrossRef\]](#)
26. Ibrahim, A.S.; Memon, F.A.; Butler, D. Seasonal variation of rainy and dry season per capita water consumption in Freetown city Sierra Leone. *Water* **2021**, *13*, 499. [\[CrossRef\]](#)
27. Vallejo, D.; Saldarriaga, J.G.; Páez, D.A.; Serrano, S. A New Methodology for the Design of Residential Water Distribution Networks and Its Population Range of Application. In Proceedings of the 11th International Conference on Hydroinformatics. HIC 2014, City University of New York (CUNY), New York, NY, USA, 17–21 August 2014. Available online: https://academicworks.cuny.edu/cc_conf_hic/95/ (accessed on 30 October 2023).
28. Trifunovic, N. *Introduction to Urban Water Distribution: Unesco-IHE Lecture Note Series*, 2nd ed.; CRC Press: Boca Raton, FL, USA, 2020.
29. Wilhelm, B.; Rapuc, W.; Amann, B.; Anselmetti, F.S.; Arnaud, F.; Blanchet, J.; Brauer, A.; Czymzik, M.; Giguet-Covex, C.; Gilli, A.; et al. Impact of warmer climate periods on flood hazard in the European Alps. *Nat. Geosci.* **2022**, *15*, 118–123. [\[CrossRef\]](#)
30. Ghimire, U.; Piman, T.; Shrestha, M.; Aryal, A.; Krittasudthacheewa, C. Assessment of Climate Change Impacts on the Water, Food, and Energy Sectors in Sittoung River Basin, Myanmar. *Water* **2022**, *14*, 3434. [\[CrossRef\]](#)
31. Heeter, K.J.; Harley, G.L.; Abatzoglou, J.T.; Anchukaitis, K.J.; Cook, E.R.; Coulthard, B.L.; Dye, L.A.; Homfeld, I.K. Unprecedented 21st-century heat across the Pacific Northwest of North America. *NPJ Clim. Atmos. Sci.* **2023**, *6*, 5. [\[CrossRef\]](#)
32. Kalbusch, A.; Henning, E.; Brikalski, M.P.; de Luca, F.V.; Konrath, A.C. Impact of coronavirus (COVID-19) spread-prevention actions on urban water consumption. *Resour. Conserv. Recycl.* **2020**, *163*, 105098. [\[CrossRef\]](#)
33. Nemati, M.; Tran, D. The impact of COVID-19 on urban water consumption in the United States. *Water* **2022**, *14*, 3096. [\[CrossRef\]](#)
34. Gholami, F.; Dehghanifard, E.; Hosseini-Baharanchi, F.S.; Gholami, M. The Quantitation of the Impact of COVID-19 Pandemic on Water Demand through GEE Modeling, a Case Study in Iran. *Case Stud. Chem. Environ. Eng.* **2023**, *8*, 100440. [\[CrossRef\]](#)
35. Buurman, J.; Freiburghaus, M.; Castellet-Viciano, L. The Impact of COVID-19 on Urban Water Use: A Review. *Water Supply* **2022**, *22*, 7590–7602. [\[CrossRef\]](#)
36. Birisci, E.; Ramazan, Ö.Z. Household Water Consumption Behavior during the COVID-19 Pandemic and Its Relationship with COVID-19 Cases. *Environ. Res. Technol.* **2021**, *4*, 391–397. [\[CrossRef\]](#)
37. Sharma, S.K. A novel approach on water resource management with Multi-Criteria Optimization and Intelligent Water Demand Forecasting in Saudi Arabia. *Environ. Res.* **2022**, *208*, 112578. [\[CrossRef\]](#) [\[PubMed\]](#)
38. United Nations. *World Population Prospects 2022: Summary of Results*. Department of Economic and Social Affairs, Population Division; UN DESA/POP/2022/TR/NO. 3; United Nations: New York, NY, USA, 2022.
39. Kowalski, D.; Suchorab, P. The Impact Assessment of Water Supply DMA Formation on the Monitoring System Sensitivity. *Appl. Sci.* **2023**, *13*, 1554. [\[CrossRef\]](#)
40. Trifunovic, N. *Introduction to Urban Water Distribution: Unesco-IHE Lecture Note Series*, 1st ed.; CRC Press: Boca Raton, FL, USA, 2006.
41. Cunha, M.C.; Sousa, J. Robust Sizing of Water Distribution Systems. In *Climate Change and Water and Energy Management in Supply and Drainage Systems*; Ramos, H.M., Covas, D.I., Gonçalves, F.V., Soares, A.K., Eds.; IST: Lisbon, Portugal, 2008; Chapter 4; pp. 260–268.
42. Lansey, K.E.; Duan, N.; Mays, L.W.; Tung, Y.K. Water Distribution System Design under Uncertainties. *J. Water Resour. Plan. Manag.* **1989**, *115*, 630–645. [\[CrossRef\]](#)
43. Xu, C.; Goulter, I.C. Reliability-Based Optimal Design of Water Distribution Networks. *J. Water Resour. Plann. Manag.* **1999**, *125*, 352–362. [\[CrossRef\]](#)
44. Kirkpatrick, S. *Optimization by Simulated Annealing: Quantitative Studies*; IBM Thomas J. Watson Research Division: Yorktown Heights, NY, USA, 1983.
45. Kirkpatrick, S.; Gelatt, C.D., Jr.; Vecchi, M.P. Optimization by simulated annealing. *Science* **1983**, *220*, 671–680. [\[CrossRef\]](#)
46. Kirkpatrick, S. Optimization by simulated annealing: Quantitative studies. *J. Stat. Phys.* **1984**, *34*, 975–986. [\[CrossRef\]](#)
47. Černý, V. Thermodynamical approach to the traveling salesman problem: An efficient simulation algorithm. *J. Optim. Theory Appl.* **1985**, *45*, 41–51. [\[CrossRef\]](#)
48. van Laarhoven, P.J.M.; Aarts, E.H.L. Simulated annealing. In *Simulated Annealing: Theory and Applications*; Mathematics and Its Applications; Springer: Dordrecht, The Netherlands, 1987; Volume 37. [\[CrossRef\]](#)
49. Millán-Páramo, C.; Matoski, A.; Mazer, W. Modified Simulated Annealing Algorithm for Optimal Design of Reinforcements with Continuous Variables. *Technol. Marcha* **2017**, *30*, 142–157. [\[CrossRef\]](#)
50. Naidu, M.N.; Boindala, P.S.; Vasan, A.; Varma, M.R. Optimization of Water Distribution Networks Using Cuckoo Search Algorithm. In *Advanced Engineering Optimization through Intelligent Techniques*; Springer: Singapore, 2020; pp. 67–74.

51. Beker, B.A.; Kansal, M.L. Complexities of the urban drinking water systems in Ethiopia and possible interventions for sustainability. *Environ. Dev. Sustain.* **2023**, *26*, 4629–4659. [CrossRef] [PubMed]
52. Ramos, H.M.; Kuriqi, A.; Besharat, M.; Creaco, E.; Tasca, E.; Coronado-Hernández, O.E.; Pienika, R.; Iglesias-Rey, P. Smart Water Grids and Digital Twin for the Management of System Efficiency in Water Distribution Networks. *Water* **2023**, *15*, 1129. [CrossRef]
53. Dieter, C.A. Water Availability and Use Science Program: Estimated Use of Water in the United States in 2015; Geological Survey. 2018. Available online: <https://pubs.usgs.gov/circ/1441/circ1441.pdf> (accessed on 7 December 2023).
54. DeOreo, W.B.; Mayer, P.; Dziegielewski, B.; Kiefer, J. *Residential End Uses of Water*, Version 2 (Executive Report) ed; Water Research Foundation: Denver, CO, USA, 2016. Available online: https://www.awwa.org/Portals/0/AWWA/ETS/Resources/WaterConservationResidential_End_Uses_of_Water.pdf (accessed on 16 January 2024).
55. Song, Z.; Jia, S. Municipal Water Use Kuznets Curve. *Water Resour. Manag.* **2023**, *37*, 235–249. [CrossRef]
56. Richter, B.D.; Benoit, K.; Dugan, J.; Getacho, G.; LaRoe, N.; Moro, B.; Rynne, T.; Tahamtani, M.; Townsend, A. Decoupling Urban Water Use and Growth in Response to Water Scarcity. *Water* **2020**, *12*, 2868. [CrossRef]
57. Fillion, Y.R.; Adams, B.J.; Karney, B.W. Stochastic design of water distribution systems with expected annual damages. *J. Water Resour. Plann. Manag.* **2007**, *133*, 244–252. [CrossRef]
58. Saldarriaga, J.G.; Serna, M.A. Resilience analysis as part of optimal cost design of water distribution networks. In Proceedings of the World Environmental and Water Resources Congress, Tampa, FL, USA, 15–19 May 2007; Restoring Our Natural Habitat; pp. 1–12.
59. González, L.; Saldarriaga, J.G. Analysis of Drinking Water Distribution Networks Based on Changes in Population Density and Topological Characteristics. In Proceedings of the World Environmental and Water Resources Congress, Atlanta, Georgia, 5–8 June 2022; pp. 913–922.
60. Balacco, G.; Carbonara, A.; Gioia, A.; Iacobellis, V.; Piccinni, A.F. Evaluation of Peak Water Demand Factors in Puglia (Southern Italy). *Water* **2017**, *9*, 96. [CrossRef]
61. Shrivastava, M.; Prasad, V.; Khare, R. Optimization Techniques for Water Supply Network: A Critical Review. *Int. J. Mech. Eng. Technol.* **2014**, *5*, 417–426.
62. Atef, A.; Osman, H.; Moselhi, O. Towards Optimum Condition Assessment Policies for Water and Sewer Networks. In *Construction Research Congress 2010: Innovation for Reshaping Construction Practice*; American Society of Civil Engineers: Reston, VA, USA, 2010; pp. 666–675. [CrossRef]
63. Marlow, D.R.; Beale, D.J.; Burn, S. 2.16—Sustainable Infrastructure Asset Management for Water Networks. In *Comprehensive Water Quality and Purification*; Ahuja, S., Ed.; Elsevier: Waltham, MA, USA, 2014; pp. 295–315. [CrossRef]
64. Wu, W.; Gao, J. Enhancing the reliability and security of urban water infrastructures through intelligent monitoring, assessment, and optimization. In *Intelligent Infrastructures*; Springer: Dordrecht, The Netherlands, 2009; pp. 487–516.
65. Kang, D.; Lansey, K. Multiperiod planning of water supply infrastructure based on scenario analysis. *J. Water Resour. Plann. Manag.* **2014**, *140*, 40–54. [CrossRef]
66. Noll, M. Exponential Life-Threatening Rise of the Global Temperature. Department of Molecular Life Sciences, Winterthurerstr, Zürich, Switzerland. *EarthArXiv* **2023**. Available online: <https://eartharxiv.org/repository/object/5420/download/10660/> (accessed on 10 January 2024).
67. National Geographic, Spain. Ciencia 2021. Available online: <https://bit.ly/3OiTKIO> (accessed on 4 December 2023).
68. Vidal, O. The Rise in the Planet’s Temperature in Three Charts. *La Vanguardia* 2021. Available online: <https://bit.ly/499myFy> (accessed on 25 October 2023).
69. Phillips, J.; Durand-Morat, A.; Nalley, L.L.; Graterol, E.; Bonatti, M.; de la Pava, K.L.; Yang, W. Understanding demand for broken rice and its potential food security implications in Colombia. *J. Agric. Food Res.* **2024**, *15*, 100884. [CrossRef]
70. Romero-Oliva, O.J. Revisión del Crecimiento Poblacional Humano y Sus Tendencias. *Con-Ciencia Boletín Científico de la Escuela Preparatoria No. 3*; 2023; Volume 10, pp. 41–43. Available online: <https://repository.uaeh.edu.mx/revistas/index.php/prepa3/article/view/10443> (accessed on 12 January 2024).
71. IBNET. 4.7—Residential Consumption (Liters/Person/Day) 2024. Available online: <https://database.ib-net.org/> (accessed on 6 January 2024).
72. Zhou, S.L.; McMahon, T.A.; Walton, A.; Lewis, J. Forecasting daily urban water demand: A case study of Melbourne. *J. Hydrol.* **2000**, *236*, 153–164. [CrossRef]
73. Haque, M.M.; Rahman, A.; Hagare, D. Impact of climate change on future water demand. *Water: J. Aust. Water Assoc.* **2014**, *41*, 57–62.
74. El-Rawy, M.; Batelaan, O.; Al-Arifi, N.; Alotaibi, A.; Abdalla, F.; Gabr, M.E. Climate change impacts on water resources in arid and semi-arid regions: A case study in Saudi Arabia. *Water* **2023**, *15*, 606. [CrossRef]

Disclaimer/Publisher’s Note: The statements, opinions and data contained in all publications are solely those of the individual author(s) and contributor(s) and not of MDPI and/or the editor(s). MDPI and/or the editor(s) disclaim responsibility for any injury to people or property resulting from any ideas, methods, instructions or products referred to in the content.